

CERN-TH.6822/93
UCLA 93/TEP/24

Cosmic Ray Signatures of Multi-W Processes

D.A. Morris*

University of California, Los Angeles
405 Hilgard Ave., Los Angeles, CA 90024, U.S.A.

A. Ringwald†

Theory Division, CERN
CH-1211 Geneva 23, Switzerland

Abstract

We explore the discovery potential of cosmic ray physics experiments for Standard Model processes involving the nonperturbative production of $\gtrsim \mathcal{O}(\alpha_W^{-1}) \simeq 30$ weak gauge bosons. We demonstrate an experimental insensitivity to proton-induced processes and emphasize the importance of neutrino-induced processes. The Fly's Eye currently constrains the largest region of parameter space characterizing multi-W phenomena if a cosmic neutrino flux exists at levels suggested by recent models of active galactic nuclei. MACRO (DUMAND) can constrain or observe additional regions by searching for 1–100 (1–10) characteristic near-vertical (near-horizontal) spatially compact energetic muon bundles per year.

CERN-TH.6822/93

UCLA 93/TEP/24

August 1993

*morris@uclahep.physics.ucla.edu

†ringwald@cernvm.cern.ch

1 Introduction

Lowest-order perturbative calculations in the Standard Model for processes involving the production of $\gtrsim \mathcal{O}(\alpha_W^{-1}) \simeq 30$ weak gauge bosons suggest an explosive (and unitarity violating) growth of the associated parton-parton cross section above center-of-mass energies $\gtrsim \mathcal{O}(\alpha_W^{-1} M_W) \simeq 2.4$ TeV [1-6]. Not surprisingly, this intriguing circumstance has drawn considerable interest in attempts to either substantiate or dismiss the possibility that the lowest-order result is a harbinger of spectacularly rich phenomena which may be observable at the next generation of hadron colliders (see ref. [7] for an overview). When unitarity is restored (most likely due to nonperturbative effects) it is conceivable that the cross section for multi-W phenomena¹ is unobservably small. However, despite concentrated theoretical efforts toward resolving the issue of large versus small cross sections [8], no definitive answer has arisen; there is a very real possibility that the question may first be settled experimentally. Given the stakes involved, a quantitative consideration of experimental constraints on multi-W production is clearly desirable.

The high-energy, high-luminosity environment of hadron colliders such as the proposed Large Hadron Collider (LHC) and the Superconducting Super Collider (SSC) would be ideal for observing or constraining multi-W phenomena over a wide range of energies and cross sections [9, 10]. However, until such machines are commissioned, cosmic rays provide the only access to the required energy scales. In this paper we adopt a purely phenomenological approach and explore the feasibility of discovering or constraining multi-W phenomena in the context of cosmic rays. We consider both atmospheric and underground phenomena induced by cosmic ray protons and neutrinos. Some of the consequences of neutrino-induced phenomena for future underwater detectors such as DUMAND [11] and NESTOR [12] have already been

¹It is understood in the following that by ‘multi-W’ phenomena we refer to processes producing a total of $\gtrsim \mathcal{O}(\alpha_W^{-1}) \simeq 30$ W’s and Z’s.

discussed in refs. [13, 14].

By adopting a simple parameterization of multi-W phenomena on the parton level, we evaluate the discovery potential of various experimental arrangements over a space of possible theories involving multi-W production. We demonstrate that even if proton-induced atmospheric multi-W phenomena occur in Nature, the features of the resulting air showers are unlikely to allow one to distinguish them from fluctuations in a much larger background of generic showers. On the other hand, ultrahigh energy neutrinos, for which a sizeable flux has recently been conjectured from sources such as active galactic nuclei [15-18], offer exciting possibilities for observing or constraining multi-W phenomena. Subsurface detectors such as AMANDA [19], DUMAND, MACRO [20], NESTOR, and NT-200 [21] can be sensitive to neutrino-induced multi-W phenomena in some regions of multi-W parameter space.

The structure of the paper is as follows. In sect. 2 we characterize multi-W phenomena by a two-parameter working hypothesis which frees us from specifying an underlying (most likely nonperturbative) mechanism for multi-W production. We also describe the gross features of multi-W phenomena and present discovery limits for the LHC and SSC. We discuss proton-induced and neutrino-induced multi-W phenomena in sects. 3 and 4, respectively. In each section we consider a variety of detection techniques and present discovery limits which may be contrasted with the superior sensitivity of future hadron colliders. In sect. 5 we summarize our results and conclude. In an appendix we outline our quantitative description of multi-W processes.

2 Working Hypothesis

In the absence of a reliable first-principles calculation of multi-W production, we adopt a working hypothesis which allows us to parametrize the essential features of nonperturbative phenomena without committing our-

selves to a specific underlying mechanism. We model the parton-parton cross section for multi-W production by

$$\hat{\sigma}_{\text{multi-W}} = \hat{\sigma}_0 \Theta(\sqrt{\hat{s}} - \sqrt{\hat{s}_0}). \quad (1)$$

For the purposes of this paper a parton is any weakly interacting particle (for example, q, ν, e). The Θ -function in eq. 1 embodies an idealized onset of nonperturbative multi-W production above a parton-parton center-of-mass threshold energy of $\sqrt{\hat{s}_0}$ with a cross section of $\hat{\sigma}_0$. While these definitions are convenient, it should be kept in mind that the true behaviour of the parton-parton multi-W cross section near threshold may be more complicated than eq. 1; in that case $\sqrt{\hat{s}_0}$ and $\hat{\sigma}_0$ in eq. 1 should be interpreted as effective parameters.

We wish to explore the possibility of observing multi-W phenomena characterized by parameters in the range

$$\begin{aligned} \frac{m_W}{\alpha_W} \simeq 2.4 \text{ TeV} &\leq \sqrt{\hat{s}_0} \leq 40 \text{ TeV}, \\ \frac{\alpha_W^2}{m_W^2} \simeq 100 \text{ pb} &\leq \hat{\sigma}_0 \leq \sigma_{\text{inel}}^{pp} \times \left(\frac{1 \text{ GeV}}{m_W}\right)^2 \simeq 10 \mu\text{b}. \end{aligned} \quad (2)$$

The lower limit of $\sqrt{\hat{s}_0}$ is suggested by the energy scale at which perturbation theory becomes unreliable [4, 5, 8] whereas the upper range is of the order of the sphaleron mass [22]. The lower range of $\hat{\sigma}_0$ follows from dimensional arguments, being characteristic of a geometrical “weak” cross section. The upper range of $\hat{\sigma}_0$ is a geometrical “strong” cross section suggested by analogies between the weak SU(2) gauge sector and the color SU(3) gauge sector [6]. Admittedly, our current theoretical understanding of weak interactions renders $\hat{\sigma}_0 \gtrsim 1 \mu\text{b}$ an unlikely scenario; we nevertheless include it in our analysis so that it may be tested experimentally. For definiteness, we will assume throughout this paper that $\hat{\sigma}_0$ refers to the production of exactly 30 W bosons; allowing for the production of variable numbers of W’s (and

Z's and possibly prompt photons) is straightforward but is an unnecessary complication at the level of our investigation.

Figure 1 shows the multi-W production cross section for protons and neutrinos (energy E) striking stationary nucleons and electrons. The curves are obtained by convoluting eq. 1 with the corresponding quark distribution functions inside nucleons (see appendix for details). The results are universal in the sense that they have been scaled by $\hat{\sigma}_0$ and $\sqrt{\hat{s}_0}$.

The simultaneous production of $\mathcal{O}(30)$ W bosons at future hadron colliders like LHC or SSC would lead to spectacular signatures [9,10]. Since the average number of charged hadrons (mainly π^\pm 's) from hadronic W decays is $\langle n_{\text{ch}}^{(W \rightarrow \text{hadrons})} \rangle \simeq 20$, one could typically expect

$$30 \times Br(W \rightarrow \text{hadrons}) \times \langle n_{\text{ch}}^{(W \rightarrow \text{hadrons})} \rangle \simeq 400 \pi^\pm \quad (3)$$

in one multi-W event accompanied by $\simeq 400$ photons from the decay of $\simeq 200 \pi^0$'s. The charged hadrons would have a minimum average transverse momentum of order

$$p_T^\pi \geq \mathcal{O}(m_W/30) \simeq (2 - 3) \text{ GeV}, \quad (4)$$

if the W bosons are produced without transverse momentum. Similarly, one could expect $\simeq 5$ prompt muons ($\simeq 3$ from W decays and $\simeq 2$ from c , b , or τ decay) carrying a minimum average transverse momentum of

$$p_T^\mu \geq \mathcal{O}(m_W/2) \simeq 40 \text{ GeV}. \quad (5)$$

A similar situation holds for other prompt leptons such as e^\pm, ν etc. It is hard to imagine that any other process in the Standard Model can mimic such a final state [10].

Figure 2 shows the regions in $\sqrt{\hat{s}_0} - \hat{\sigma}_0$ space accessible to the LHC ($\sqrt{s} = 14.6 \text{ TeV}; \mathcal{L} = 10^{34} \text{ cm}^{-2}\text{s}^{-1}$) and the SSC ($\sqrt{s} = 40 \text{ TeV}; \mathcal{L} = 10^{33} \text{ cm}^{-2} \text{ s}^{-1}$). The contours correspond to 1 and 10 events (assuming 100%

detection efficiency) for 10^7 s of operation. These contours may be used as a benchmark to evaluate the effectiveness of various cosmic ray physics experiments for constraining multi-W phenomena.

3 Proton-Induced Multi-W Processes

Cosmic ray protons and heavy nuclei constitute a guaranteed flux of high-energy primaries potentially capable of initiating multi-W phenomena. In this section we explore the possibility of exploiting this cosmic flux and isolating multi-W phenomena from generic hadronic reactions. We restrict our attention to cosmic ray protons since they provide the dominant flux in terms of energy per nucleon.

Since the flux of proton-induced multi-W air showers is anticipated to be small for even the most optimistic scenarios, one must resort to experiments with large effective areas and/or long exposure times. We will discuss three types of relevant experiments:

- 1) conventional surface arrays which measure the e, γ, μ , etc., content of air showers (AGASA [23], CYGNUS [24], CASA [25], EAS-TOP [26], EAS-100 [27], HEGRA [28], KASCADE [29], etc.),

- 2) underground experiments sensitive to downward through-going TeV muons (LVD [30], MACRO [20], Soudan-2 [31], etc.) or underwater(-ice) experiments which detect energetic muons by Cherenkov light (AMANDA [19], DUMAND [11], NESTOR [12], NT-200 [21], etc.), and

- 3) the Fly's Eye [32], an optical array which is sensitive to nitrogen fluorescence light from air showers.

3.1 Conventional surface arrays

Using a network of detector elements, conventional surface arrays reconstruct the features of an extensive air shower by interpolating or extrapolating

measurements of a shower's particle content. Among the particles sampled are photons and electrons with $E_e, E_\gamma \gtrsim \mathcal{O}(1 \text{ MeV})$, muons with $E_\mu \gtrsim \mathcal{O}(1 \text{ GeV})$, and, in some experiments, hadrons with $E_{\text{had}} \gtrsim 1 \text{ GeV}$.

Consider a surface array (area A) sensitive to showers above a threshold energy E_{thresh} . For proton-induced phenomena it follows from elementary considerations that the number of multi-W showers occurring during time t is

$$\text{Number of multi-W showers} = t A \Omega \int_{E_{\text{thresh}}}^{\infty} dE \frac{\sigma_{\text{multi-W}}^{pN}(E)}{\sigma_{\text{inel}}^{pN}(E)} j_p(E), \quad (6)$$

where $j_p(E) = dN_p/(dAdtd\Omega dE)$ is the cosmic proton flux and Ω is the solid angle acceptance of the array. For the cases we consider the inelastic proton-nucleon cross section $\sigma_{\text{inel}}^{pN}$ is dominated by generic QCD interactions and may be approximated by $\sigma_{\text{inel}}^{pN}(E) \simeq \text{const.} \simeq 100 \text{ mb}$. In principle, multi-W production through proton-electron collisions is also possible. However as illustrated in Fig. 1, the cosmic proton threshold energy for multi-W production in pe^- collisions is $m_p/m_e \simeq 1800$ times larger than the corresponding pN threshold. Moreover, the pe^- multi-W cross section is at least 100 times smaller than the pN multi-W cross section; hence we neglect multi-W production through pe^- collisions.

Figure 3 shows contours for the number of proton-induced multi-W air showers at zenith angles $\theta \leq 60^\circ$ striking a 100 km^2 conventional surface array in 10^7 s . For our calculations we use the cosmic proton flux of the Constant Mass Composition (CMC) model [33] (see Fig. 4). Though the total flux of ultrahigh energy hadronic cosmic rays is relatively well measured, its composition (*i.e.*, percentage of p, Fe, Mg etc.) is somewhat less certain. Our use of the CMC proton flux introduces an inherent, though not critical uncertainty in this respect; the CMC flux is a compromise between proton-rich [34] and proton-poor [35] scenarios. For purposes of illustration we optimistically assume $E_{\text{thresh}} = 1 \text{ PeV}$ which accommodates all multi-W thresholds

above $\sqrt{\hat{s}_0} \geq 2.4$ TeV. In 100 km² arrays like AGASA and EAS-100, inter-detector spacing on the order of .5–1 km makes $E_{\text{thresh}} = 100 - 1000$ PeV more realistic but does not change our conclusions.

Though the region of the $(\sqrt{\hat{s}_0}, \hat{\sigma}_0)$ plane accessible to surface arrays is clearly limited by the absolute rate of proton-induced multi-W phenomena, it is instructive to consider how one might distinguish an air shower of multi-W origin from a generic hadronic air shower. For the remainder of this section, we restrict our attention to the optimistic scenario of parton-parton multi-W threshold of $\sqrt{\hat{s}_0} = 2.4$ TeV with $\hat{\sigma}_0 = 10$ μb ; for this choice of parameters a 100 km² array would see approximately 110 (45) multi-W showers in 10⁷ s at zenith angles $\theta < 60^\circ$ for $E_{\text{thresh}} = 1$ PeV (100 PeV). As illustrated in Fig. 5, the combination of a rising $\sigma_{\text{multi-W}}^{pN}(E)$ with a falling cosmic proton flux spectrum implies that typical multi-W showers would have energies well above the corresponding cosmic proton threshold energy of $E_p^{\text{thresh}} = \hat{s}_0/(2m_p) \simeq 3$ PeV. The most probable shower energy is $\simeq 30$ PeV and the average shower energy is $\simeq 250$ PeV due to a long tail on the distribution.

Consider the characteristics of the most probable ($\simeq 30$ PeV) multi-W air showers. To phrase our results in experimentally relevant terms we use the computer program SHOWERSIM [36] to simulate multi-W air showers and generate samples of generic proton-induced and iron-induced showers (see appendix for details). Figure 6 compares 30 PeV multi-W, proton and iron showers in terms of radial particle densities (with respect to a vertical shower axis) of electrons ($E_e \geq 1$ MeV), muons ($E_\mu \geq 1$ GeV) and hadrons ($E_{\text{had}} \geq 1$ GeV). Each curve is averaged over 25–100 showers taking into account the distribution of the depth of first interaction in the upper atmosphere. The densities in Fig. 6 correspond to an observation depth of 800 g/cm² (roughly the CYGNUS array depth [24]). The corresponding average particle numbers are listed in Table 1. We neglect possible systematic uncertainties in the experimental determination of shower energies which may be important

in practice.

The differences between the particle density profiles of 30 PeV showers in Fig. 6 are hardly striking. While there are identifiable systematic differences between average showers of different origin, the differences do not appear to be sufficient to discriminate between multi-W showers and fluctuations in generic proton or iron showers. We emphasize this point by noting that in the CMC flux model, the differential fluxes of 30 PeV generic proton-induced, iron-induced and multi-W showers (with $\sqrt{\hat{s}_0} = 2.4$ TeV, $\hat{\sigma}_0 = 10$ μb) stand in the proportion $p : \text{Fe} : \text{multi-W} \simeq 1.2 \times 10^5 : 1.1 \times 10^5 : 1$.

Considering the spectacular underlying nature of multi-W phenomenon the similarities between proton-induced multi-W showers and generic proton and iron may appear surprising. However, a proton-induced multi-W shower is actually a superposition of an “interesting” prompt shower component seeded by the instantaneous decays of W bosons and a generic “uninteresting” component initiated by the proton fragment which does not participate in the multi-W production subprocess. The proton fragment emerges from the region of multi-W production, hadronizes, and subsequently generates a generic hadronic shower deeper in the atmosphere. Since the proton fragment typically carries a substantial fraction of the primary proton energy, the so-called leading particle effect, a large generic component to a proton-induced multi-W shower jeopardizes the chances of isolating multi-W showers from “pure” generic showers. As shown in Fig. 7, approximately 60% (20%) of the total energy in a 30 PeV (5 PeV) proton-induced multi-W air shower is carried by the generic component.

To minimize the effects of the uninteresting generic component of multi-W showers and accentuate the prompt component one may be tempted to consider multi-W showers close to the relevant threshold energy. Flatter particle densities near the core of 5 PeV multi-W showers (compared to 30 PeV showers) in Fig. 6 suggest the larger transverse momentum characteristic of particles from W decay. However, it is unlikely that one can capitalize on

such effects in practice. Due to the slow turn-on of $\sigma_{\text{multi-W}}^{pN}$ (see Fig. 1), showers just above threshold are rare; for the case at hand only .0002% (17% of proton-induced multi-W showers have energy less than 5 PeV (30 PeV). This corresponds to only one proton-induced multi-W air shower (with $E_{\text{shower}} < 5$ PeV) in a 100 km² array every 4400 years! In summary, the prospects for detecting proton-induced multi-W phenomena using conventional surface arrays are poor.

3.2 Underground detectors

In an effort to overcome the complications introduced by a large generic shower component in proton-induced multi-W air showers, it is helpful to concentrate on aspects of air showers which reflect the nature of the primary hard interaction. Energetic muons produced from the prompt decays of W bosons or from the weak decays of energetic mesons are good candidates in this respect. For definiteness, we restrict our attention to muons with $E_{\mu} > 1.5$ TeV; such muons can penetrate to deep underground detectors such as MACRO [20].

As shown in Fig. 8 the lateral distribution of TeV muons in 30 PeV multi-W showers is flatter than the corresponding distributions for 30 PeV generic p-induced or Fe-induced showers. The flatter multi-W distribution is characteristic of the large transverse momentum of the prompt muons from W (and Z) decays, eq. 5, and the decays of pions and kaons, eq. 4. The corresponding average number of TeV muons in each type of shower is given in the last column of Table 1.

Though distinct, TeV muon signatures from proton-induced multi-W phenomena are limited by small event rates and practical detector sizes. The event rate contours for MACRO can be estimated from the 100 km² surface array contours in Fig. 3 simply by scaling by the area ratio (12 m × 77 m)/100 km² $\simeq 10^{-5}$, implying negligibly small rates. Even for poorly mo-

tivated parameters such as ($\sqrt{\hat{s}_0} = 2.4$ TeV, $\hat{\sigma}_0 = 100$ μb) one would need an underground detector with an area sensitive to downward moving muons of $\mathcal{O}(10^5 \text{ m}^2)$ to see penetrating muons from one proton-induced multi-W event in 10^7 s. In view of these small rates, present and future underground detectors are not sensitive to penetrating muon signatures of proton-induced multi-W phenomena.

3.3 Fly's Eye

Finally, we turn to the discovery potential of the Fly's Eye [32], an optical array sensitive to nitrogen fluorescence light from air showers whose trajectories do not necessarily intersect the array. By detecting fluorescence light emitted as air showers streak across the sky, the Fly's Eye is capable of reconstructing the longitudinal development of air showers with energy greater than $E_{\text{thresh}} = 100$ PeV (see ref. [37] for a pedagogical introduction).

Analogous to our previous calculation for conventional arrays, the number of proton-induced multi-W showers seen in time t by the Fly's Eye is given by

$$\text{Number of multi-W showers} = t \int_{E_{\text{thresh}}}^{\infty} dE \frac{\sigma_{\text{multi-W}}^{pN}(E)}{\sigma_{\text{inel}}^{pN}(E)} j_p(E) A\Omega(E), \quad (7)$$

where the acceptance, $A\Omega$, is a function of energy and hence appears under the integral. Fig. 3 shows event number contours for proton-induced multi-W air showers corresponding to 10^7 s operation of the Fly's Eye using the CMC proton flux and the acceptance of ref. [32]. Due to its sensitivity, the Fly's Eye operates only on clear, moonless nights; approximately 2×10^6 s of observation time is possible in one calendar year [32].

Despite the limited region of multi-W parameter space accessible to the Fly's Eye through proton-induced multi-W air showers we consider whether multi-W showers, if present, can be differentiated from generic showers. In the same spirit that one expects generic Fe-induced air showers to develop

more rapidly than generic p-induced showers, one might expect that the large initial multiplicity in a multi-W event (from the immediate decay of the W bosons) leads to an accelerated development of the corresponding air shower. To test this hypothesis we compare the longitudinal profiles (*i.e.*, the number of electrons as a function of shower depth) of multi-W showers with those of generic p- and Fe-induced air showers. Fig. 9 shows samples of 150 PeV vertical showers of each type. The multi-W air showers assume a parton-parton threshold of $\sqrt{\hat{s}_0} = 5$ TeV so that 150 PeV showers are approximately a factor of 10 above the corresponding proton threshold of $\hat{s}_0/(2m_p) \simeq 13$ PeV and are not atypical; for this choice of threshold the Fly's Eye would expect to see 1–10 multi-W air showers within 10^7 s observation time for $\hat{\sigma}_0$ in the range 10-100 μb .

For ease of comparison in Fig. 9, the depth of first interaction of 150 PeV cosmic ray protons (Fe nuclei) was fixed at 42 g/cm² (11 g/cm²) which corresponds to the average depth of first interaction. While systematic differences are evident between profiles of different origin, the longitudinal profiles of multi-W showers are not sufficiently distinctive to prevent confusion with fluctuations in generic air showers. For ($\sqrt{\hat{s}_0} = 5$ TeV, $\hat{\sigma}_0 = 10$ μb) the differential fluxes of 150 PeV generic proton-induced, iron-induced and multi-W showers stand in proportion to $\simeq 80000 : 75000 : 1$ in the the CMC model.

4 Neutrino-Induced Multi-W Processes

A cosmic flux of ultrahigh energy neutrinos would provide a novel opportunity to search for multi-W phenomena. Unlike proton-induced multi-W production which must compete with $\mathcal{O}(100 \text{ mb})$ generic hadronic processes, neutrino-induced multi-W production competes only with $\mathcal{O}(\text{nb})$ weak interaction processes. Fortuitously, considerable enthusiasm has been generated recently by predictions of a large flux of cosmic neutrinos from active galactic nuclei (AGN) [15-18]. Indeed, in the model of Stecker *et al.* (see Fig. 4)

the diffuse flux of PeV neutrinos from AGN is comparable to the flux of cosmic protons in the CMC model! If only generic charged current interactions are operative, the Stecker *et al.* flux suggests that DUMAND should see 154(66) single muon events per year with energies $E_\mu \geq 100$ GeV (10 TeV) at zenith angles $\theta > 70^\circ$ [18]. In this section we explore alternatives for uncovering neutrino-induced multi-W phenomena assuming that a flux of ultrahigh energy neutrinos does, in fact, exist.

We restrict our attention to multi-W phenomena in neutrino-nucleon collisions and neglect multi-W phenomena from neutrino-electron collisions. As may be deduced from Fig. 1, the ratio $\sigma_{\text{multi-W}}^{\nu e^-} / \sigma_{\text{multi-W}}^{\nu N}$ reaches a maximum of $\simeq 1/30$ when $\sigma_{\text{multi-W}}^{\nu e^-}$ turns on. Since the number density of electrons in matter is nominally half that of nucleons, $\lesssim 1/60 \simeq 2\%$ of multi-W events are due to neutrino-electron interactions.

Concerning neutrino flux attenuation due to competing processes, we neglect generic νe^- weak interactions compared to generic νN weak interactions. In the energy range of interest the neutrino-electron cross section due to generic weak interactions is $\lesssim \mathcal{O}(5\%)$ of the corresponding generic neutrino-nucleon cross sections [38] for ν_e, ν_μ and $\bar{\nu}_\mu$. The only exception is the Glashow resonance $\bar{\nu}_e + e^- \rightarrow W^-$ at $E_{\bar{\nu}_e} \simeq 6.3$ PeV which is $\mathcal{O}(10^2 - 10^3)$ times larger than the generic $\sigma_{\bar{\nu}_e N}$ [39]. However, since $\bar{\nu}_e$ are anticipated to make up only $\mathcal{O}(1/6)$ of ultrahigh energy neutrinos of AGN origin and the Glashow resonance is relevant only near the lowest of multi-W thresholds (before $\sigma_{\text{multi-W}}^{\nu N}$ has fully turned on), we neglect this effect for multi-W production.

We divide our discussion of neutrino-induced multi-W phenomena into four sections. Given that AGN are the most plausible source of our assumed neutrino flux, we investigate in sect. 4.1 the conditions under which large neutrino cross sections for multi-W production are compatible with AGN neutrino production mechanisms. In sect. 4.2 we discuss constraints on neutrino-induced multi-W production from the Fly's Eye and in sect. 4.3 we

consider the possibility of using conventional air shower arrays. In sect. 4.4 we evaluate the potential of subsurface detectors to observe contained multi-W phenomena and discuss the detection of distant multi-W phenomena through searches for energetic muon bundles.

4.1 AGN neutrinos with large cross sections

Active galactic nuclei are natural candidates for ultrahigh energy neutrino production [40, 41]. In the AGN model of Stecker *et al.* [15] charged pions are produced in reactions such as $p\gamma \rightarrow \Delta^+ \rightarrow n\pi^+$ when protons accelerated by a spherical accretion shock [42] collide with the dense gas of ultraviolet photons in the innermost region around the central black hole. Charged pions decay and give rise to neutrinos, whereas photons produced through π^0 decay cascade to lower energies, eventually appearing as X-rays. If it is assumed that the diffuse X-ray background is primarily from AGN, the observed X-ray flux can be used to normalize the calculation of the neutrino flux. Szabo and Protheroe [16] have extended this model by including pion production through pp interactions. The AGN model by Biermann and collaborators [17] differs from the model used in refs. [15, 16] mainly in the geometry; the shocks needed for the acceleration of the protons are assumed to arise in the bipolar outflow of gas and plasma perpendicular to the accretion disc [43].

Among other considerations, prolific neutrino production by AGN is a function of the matter density in the vicinity of the pion production; if the medium is too dense, charged pions undergo subsequent hadronic interactions instead of decaying to give neutrinos. For example, for PeV pions the matter density should be less than 10^{-8} g/cm³ [18]. Assuming that the prevailing conditions are indeed conducive to neutrino production, we must consider whether or not potentially large neutrino-induced multi-W cross sections permit produced neutrinos to escape. For example, one might worry about

neutrino reabsorption due to multi-W phenomena through collisions with the dense gas of ultraviolet photons required by the AGN model of Stecker *et al.* However, even a low parton-parton multi-W threshold of $\sqrt{\hat{s}_0} = 2.4$ TeV corresponds to a neutrino threshold energy (colliding with $\simeq 40$ eV photons) of 3×10^{13} GeV; we can safely ignore this effect. More important is the effect of neutrino reabsorption by matter; the relevant parameter is the column density seen by particles escaping from the inner regions of AGN.

In the Stecker *et al.* model the effective escape column density for neutrinos from the central region of the AGN is of the order of the column density of the X-ray emitting region, $X_{\text{escape}}^{\text{Stecker } et al.} \simeq X_{\text{X-ray}} \simeq \mathcal{O}(10^{-3} - 10^{-1} \text{ g/cm}^2)$ [15, 45] whereas in the model of Biermann *et al.* $X_{\text{escape}}^{\text{Biermann } et al.} \simeq 10^2 \text{ g/cm}^2$ is of the order of a hadronic interaction length [46]. As can be seen in Fig. 10 which plots the neutrino interaction length $X_\nu = m_p / \sigma_{\text{multi-W}}^{\nu N}(E_\nu)$, significant reabsorption of neutrinos by AGN is not an issue since $X_\nu \gg X_{\text{escape}}$. A related point, but one which we do not address in this paper, is the implication of large neutrino cross sections for stars near the cores of AGN. Neutrino interaction lengths of $\mathcal{O}(10^9 \text{ g/cm}^2)$ due to generic charged currents for $E_\nu \simeq 1 - 100$ PeV are sufficient to disrupt stellar evolution near the cores of AGN [47, 15]; shorter neutrino interaction lengths implied by multi-W phenomena may have interesting consequences.

For definiteness, we use the (revised) Stecker *et al.* AGN neutrino flux [15] in the following sections for estimates of expected rates of multi-W phenomena. It should be noted, however, that the fluxes calculated in refs. [16, 17] generally agree² with Stecker *et al.* [15] above .1 PeV, which is the energy range we are interested in. In this sense our use of the Stecker *et al.* flux is intended to be representative of a large class of AGN flux models.

²At lower energies refs. [16, 17], which take *pp* interactions into account, give considerably larger fluxes than ref. [15] (see, *e.g.*, Fig. 11 in ref. [18])

4.2 The Fly’s Eye experiment

Independent of any neutrino flux model, the Fly’s Eye array [32] puts upper limits on the product of the flux times total cross section for weakly interacting particles in the range $10^8 \text{ GeV} \leq E_\nu \leq 10^{11} \text{ GeV}$ assuming that such particles initiate extensive air showers deep in the atmosphere [48]. The limits are deduced from the non-observation of downward-moving air showers within the Fly’s Eye fiducial volume such that the shower axis is inclined 80° to 90° from the zenith at the point of impact on the Earth. Showers meeting these criteria could only have been initiated by particles typically penetrating more than 3000 g/cm^2 of atmosphere before interacting, which excludes showers initiated by ultrahigh energy photons and hadrons.

Assuming that the weakly interacting particles referred to by the Fly’s Eye are neutrinos, we denote the relevant cross section by $\sigma_{\text{tot}}^{\nu N}(E_\nu)$ which receives contributions from both multi-W and familiar charged current weak interactions. The Fly’s Eye limits may be summarized by $(j_\nu \sigma_{\text{tot}}^{\nu N})_{\text{Fly's Eye}} \leq 3.74 \times 10^{-42} \times (E_\nu/1 \text{ GeV})^{-1.48} \text{ s}^{-1} \text{ sr}^{-1} \text{ GeV}^{-1}$ [13, 49]. Since these limits neglect the possibility of flux attenuation in the upper atmosphere due to large inelastic cross sections, they nominally apply only if $\sigma_{\text{tot}}^{\nu N}(E_\nu) \leq 10 \text{ } \mu\text{b}$. If one considers a particular neutrino flux model $j_\nu^{\text{model}}(E_\nu)$ the Fly’s Eye limit excludes regions in the $(E_\nu, \sigma_{\text{tot}}^{\nu N})$ plane bounded by

$$\frac{(j_\nu \sigma_{\text{tot}}^{\nu N})_{\text{Fly's Eye}}}{j_\nu^{\text{model}}} < \sigma_{\text{tot}}^{\nu N}(E_\nu) < 10 \text{ } \mu\text{b}, \quad (8)$$

$$10^8 \text{ GeV} < E_\nu < 10^{11} \text{ GeV}.$$

If we use the AGN neutrino flux of Stecker *et al.* [15] (i.e., set $j_\nu^{\text{model}} = j_\nu^{\text{Stecker et al.}}$), the Fly’s Eye excludes the hatched region of Fig. 11.

In order that $\sigma_{\text{tot}}^{\nu N}(E_\nu)$ avoid the region excluded by eq. 8, only certain combinations of $\sqrt{\hat{s}_0}$ and $\hat{\sigma}_0$ are consistent. For example, as shown in Fig. 11, for $\sqrt{\hat{s}_0} = 8 \text{ TeV}$ the range $.5 \text{ } \mu\text{b} < \hat{\sigma}_0 < 81 \text{ } \mu\text{b}$ is excluded. Similar consid-

erations for other values of $\sqrt{\hat{s}_0}$ result in the excluded region labeled “AGN ν ” in Figure 12. As may be quickly verified, the upper left boundary of the excluded region in Figure 12 corresponds to limiting situations in which $\sigma_{\text{tot}}^{\nu N}(E_\nu = 10^8 \text{ GeV}) = 10 \mu\text{b}$. In principle the $10 \mu\text{b}$ upper bound on the neutrino-nucleon cross section in eq. 8 could be enlarged by taking into account flux attenuation in the upper atmosphere, which has been neglected in ref. [48]. As a consequence, one could most likely extend the excluded region in Fig. 12 into the upper left hand corner which, taken literally, is not constrained by the Fly’s Eye. A further improvement of the Fly’s Eye limit $(j_\nu \sigma_{\text{tot}}^{\nu N})_{\text{Fly’s Eye}}$, by a factor of 10–50, is expected from the High Resolution (HiRes) Fly’s Eye [50].

Active galactic nuclei are not the only conjectured sources of ultrahigh energy neutrinos. As shown in Fig. 4, when the proposed AGN neutrino flux dies off beyond $\simeq 1 \text{ EeV}$, the dominant component to the neutrino flux may be due to protons scattering inelastically off the 2.7 K cosmic background radiation (CBR) [51], producing charged pions that subsequently decay and produce neutrinos [52, 53]. The photoproduced neutrino flux, $j_\nu^{2.7 \text{ K}}$, shown in Fig. 4 is taken from ref. [15]. It is amusing to consider how the Fly’s Eye constraints on neutrino-induced multi-W production are modified if we account for the possibility of such photoproduced neutrinos. If one takes $j_\nu^{\text{model}} = j_\nu^{\text{Stecker et al.}} + j_\nu^{2.7 \text{ K}}$ in eq. 8, the Fly’s Eye excludes the $(E_\nu, \sigma_{\text{tot}}^{\nu N})$ region shown Fig. 13 and enlarges the excluded region in $(\sqrt{\hat{s}_0}, \hat{\sigma}_0)$ space by the area labelled “2.7 K Photoproduced ν ” in Fig. 12.

Though the appearance of an enlarged excluded region is welcome, it is sensitive to details of the assumed CBR flux. Had we assumed a CBR flux component $j_\nu^{2.7 \text{ K}}$ which was a factor of ten smaller than that shown in Fig. 4 (corresponding to a lower redshift), the quantity $(j_\nu \sigma_{\text{tot}}^{\nu N})_{\text{Fly’s Eye}}/j_\nu^{\text{model}}$ (corresponding to the solid curve in Fig. 13) would not have dipped below $10 \mu\text{b}$ and thus would not have introduced a constraint. We should keep such uncertainties in mind to avoid attaching undue significance to the excluded

regions in Fig. 12. Nevertheless it is intriguing to speculate about detecting CBR neutrinos via multi-W processes since the prospects for detecting such neutrinos through generic weak interactions is poor unless the CBR neutrino flux is associated with a very large redshift.

4.3 Conventional air shower arrays

Consider a conventional air shower array (area A) which is located at an atmospheric depth X_0 and is sensitive to showers above a threshold E_{thresh} . For showers not close to the horizon it is straightforward to show that the number of multi-W showers in time t occurring in the atmosphere above the detector is

$$\text{Number of multi-W showers} = \frac{t A}{m_p} \int_{E_{\text{thresh}}}^{\infty} dE d\Omega \frac{X_0}{\cos \theta} \sigma_{\text{multi-W}}^{\nu N}(E) j_{\nu}(E). \quad (9)$$

The solid contours of Figure 14 correspond to neutrino-induced multi-W events in 10^7 s above a 100 km^2 array which is sensitive to showers above 100 PeV within 60° of the zenith; the AGN neutrino flux of Stecker *et al.* [15] has been assumed. Even though the neutrino flux is smaller than the cosmic proton flux in the CMC model (see Fig. 4) the contours for neutrino-induced multi-W phenomena cover a considerably larger region in the $\sqrt{\hat{s}_0} - \hat{\sigma}_0$ plane than the corresponding contours for proton-induced air showers (see Fig. 3). This is due to a more rapid growth of the multi-W cross section for νN scattering compared to pN scattering (Fig. 1) and also due to a much smaller competing cross section from generic charged current interactions, $\sigma_{\text{c.c.}}^{\nu N} \simeq \mathcal{O}(1 \text{ nb})$.

The solid contours in Fig. 14 do not account for the efficiency of an array to trigger on low altitude air showers. Such considerations are crucial for neutrino-induced phenomena since the distribution of neutrino interactions essentially follows the density profile of the atmosphere. In an exponential at-

mosphere neutrino-induced air showers may be initiated so close to the array that the showers do not spread out sufficiently to trigger the array. Rather than confine ourselves to a detailed analysis of triggering requirements, consider the following approximation. Suppose that an array does not trigger on showers initiated with 500 g/cm^2 of the detection level. This assumption is reasonable for vertical showers but is somewhat pessimistic for showers at larger zenith angles. Contours for “triggerable” neutrino-induced multi-W air showers follow from eq. 9 if, in the integrand, we replace $X_0/\cos\theta$ with $(X_0/\cos\theta - 500 \text{ g/cm}^2)$.

The dashed contours of Fig. 14 correspond to “triggerable” neutrino-induced multi-W showers. It is interesting to note that the contours for $\simeq 5 - 10$ events in 10^7 s for a 100 km^2 surface array roughly coincide with the lower boundary of the Fly’s Eye excluded region labelled “AGN ν ” in Fig. 12; this effect is easily understood in terms of the relevant acceptances and exposure times. If, in addition to the AGN neutrino flux of Stecker *et al.*, we were to assume contributions from 2.7 K photoproduced neutrinos as in the previous section, we would find contours for $\mathcal{O}(1)$ event in 10^7 s for a 100 km^2 surface array which roughly coincide with the lower boundary of the Fly’s Eye excluded region labelled “2.7 K Photoproduced ν ” in Fig. 12. In other words, assuming the same neutrino flux, the sensitivity of the Fly’s Eye to multi-W phenomena is comparable to that of a 100 km^2 surface array. For this reason we will not discuss the characteristics of neutrino-induced multi-W air showers relevant to surface arrays. Mrenna [54] has compared the features of neutrino-induced air showers and generic air showers in the context of composite models [55] where hypothesized colored subconstituents of PeV neutrinos interact with typical QCD cross sections.

Conventional air shower arrays can also search for showers close to the horizon. Data from the AKENO array places limits on the existence of electromagnetic (muon-poor) horizontal air showers initiated deep in the atmosphere [56, 57]. Since the AKENO data applies only to shower energies lower

than the multi-PeV range in which we are interested [58], we have not investigated its implications for multi-W phenomena. Exploitation of the horizontal shower limits would require consideration of distant neutrino-induced multi-W processes in which only prompt muons penetrate the intervening atmosphere and initiate electromagnetic cascades close the surface array.

4.4 Subsurface experiments

Detectors deep below the surface of the Earth, be they shielded by rock (LVD [30], MACRO [20], Soudan-2 [31] etc.), water (DUMAND [11], NESTOR [12], NT-200 [21]) or ice (AMANDA [19]) offer a unique perspective on neutrino-induced phenomena. In this section we investigate two possible modes for detecting neutrino-induced multi-W phenomena using subsurface experiments. We first consider the prospects for observing contained neutrino-induced multi-W phenomena and later turn to the detection of muon bundles arising from neutrino interactions in the surrounding medium.

Aside from the energy involved, contained neutrino-induced multi-W production would reveal its origins by its enormous multiplicity ($\mathcal{O}(400)$ charged hadrons, $\mathcal{O}(400)$ photons, and a few prompt muons and electrons). Generic deep inelastic νN scattering and the resonant process $\bar{\nu}_e + e^- \rightarrow W^- \rightarrow$ hadrons can also give contained hadron production, but only with significantly lower multiplicity.

The number of neutrino-induced multi-W events occurring inside a subsurface detector volume V during a time t is

$$\text{Number of multi-W events} = t \frac{\rho V}{m_p} \sigma_{\text{multi-W}}^{\nu N} \int dE_\nu d\Omega j_\nu(E_\nu) e^{-\sigma_{\text{tot}}^{\nu N} X(\theta, \phi)/m_p}, \quad (10)$$

where $X(\theta, \phi)$ is the column density of material in the (θ, ϕ) direction between the detector and the upper atmosphere and ρ is the density of the material in which the neutrino interaction occurs.

Figure 15 shows contours for contained multi-W events in 10^7 s in a 1 km^3 volume of water at an ocean depth of 4.5 km. This arrangement approximates the proposed SADCO acoustic array [59] which, though designed to use acoustic techniques to detect the resonant process $\bar{\nu}_e + e^- \rightarrow W^-$, would also be sensitive to multi-W phenomena which are more energetic. Acoustic techniques have also been considered for AMANDA [60] and DUMAND [61]. The contours in Fig. 15 consider the AGN neutrino flux of Stecker *et al.* [15] as well as the sum of the Stecker flux with the 2.7 K photoproduced component from Fig. 4.

Contours for the number of contained multi-W events in DUMAND can be obtained from Fig. 15 simply by scaling the appropriate volume ratio. If we idealize DUMAND as a $100 \text{ m} \times 100 \text{ m} \times 250 \text{ m}$ volume under 4.5 km of water (neglecting the possibility that its effective acoustic volume can be larger than its geometrical size), the volume ratio is $\simeq 1/400$. Due to a numerical coincidence, the corresponding contours for MACRO (which we idealize as a $77 \text{ m} \times 12 \text{ m} \times 9 \text{ m}$ volume at a depth of 3700 hg/cm^2 below the surface of a spherical Earth with $\rho = 2.6 \text{ g/cm}^3$) may be obtained by from Fig. 15 by scaling by a factor of $\simeq 1/40000$, implying MACRO's insensitivity to contained events.

Due to the enormous energies involved, one need not to concentrate on completely contained multi-W reactions. Of particular interest is the ability for subsurface detectors to detect muons which arise from energetic neutrino interactions up to a few kilometers away. For distant multi-W production the effects of producing hundreds of hadrons and photons will have died off well before reaching the detector but the anticipated 2–3 muons from prompt W decays produced with $E_\mu \simeq \mathcal{O}(100 \text{ TeV})$ and $p_T^\mu \simeq \mathcal{O}(40 \text{ GeV})$ propagate great distances. The signature of multi-W production in this case would be energetic muon bundles.

The ability to detect muons from distant neutrino reactions increases a subsurface detector's effective neutrino target volume dramatically and is the

premise upon which such detectors can act as neutrino telescopes. Considerable effort has recently been directed towards the prospects of detecting ultrahigh energy neutrinos (most likely from AGN) using subsurface detectors [18]. Despite their limited sensitivity to such phenomena, Fréjus [62] and Soudan-2 [63] have already placed useful observational constraints on AGN flux models.

As discussed in ref. [13], near-horizontal muon bundles in DUMAND and MACRO would be characteristic of neutrino-induced multi-W phenomena. By concentrating on large zenith angles, one can avoid the complications from a large background of muon bundles from generic hadronic interactions in the atmosphere. The number of muon bundles containing k muons detected during time t by a subsurface detector of length L , width W and height H is

$$\text{Number of muon bundles} = t \times \int d \cos \theta \frac{dN_{k\mu}}{dA dt d\Omega} \left[\frac{2}{\pi} H(L+W) \sin \theta + LW |\cos \theta| \right], \quad (11)$$

where the quantity in square brackets is the azimuthally averaged projected area of the detector. The calculation of the differential flux of muon bundles containing k muons, $dN_{k\mu}/(dA dt d\Omega)$, employs the techniques of ref. [13] which are summarized in the appendix.

We present in Fig. 16 contours for muon bundles beyond zenith angles of 80° for MACRO and DUMAND for the AGN neutrino flux of Stecker *et al.* [15]. Due to our assumed production of 30 W bosons, each muon bundle consists of approximately 3 muons. The average muon energy $\langle E_\mu \rangle$ entering the detector and the average inter-muon separation $\langle r_\mu \rangle$ depend on $\sqrt{\hat{s}_0}$ and $\hat{\sigma}_0$. For example, for $(\sqrt{\hat{s}_0} = 4 \text{ TeV}, \hat{\sigma}_0 = 10 \text{ nb})$ one expects $\simeq 1.5$ bundles per 10^7 s in DUMAND with $\langle E_\mu \rangle \simeq \mathcal{O}(180 \text{ TeV})$ and $\langle r_\mu \rangle = \mathcal{O}(2.5 \text{ m})$; for $(\sqrt{\hat{s}_0} = 4 \text{ TeV}, \hat{\sigma}_0 = 1 \mu\text{b})$ one expects $\simeq 30$ bundles per 10^7 s in DUMAND with $\langle E_\mu \rangle \simeq \mathcal{O}(70 \text{ TeV})$ and $\langle r_\mu \rangle = \mathcal{O}(3.6 \text{ m})$. Assuming an additional 2.7 K photoproduced neutrino flux component at the level shown in Fig. 4 changes the contours of Fig. 16 by a negligible amount.

It may also be possible to constrain multi-W phenomena by searching for non-horizontal muon bundles and thereby enlarge the accessible region in $\sqrt{\hat{s}_0}-\hat{\sigma}_0$ space. Fig. 17 (Fig. 18) shows contours for muon bundles for zenith angles between 0° and 180° for DUMAND (MACRO³) for the Stecker *et al.* AGN neutrino flux. An additional 2.7 K photoproduced neutrino flux component at the level of fig. 4 changes the 1-10 event contours for DUMAND but has a negligible effect on the MACRO contours. Since DUMAND is specifically not optimized for downward muons the DUMAND rates in Fig. 17 are presented as a matter of completeness rather than practicality. MACRO, however, is sensitive to downward muons. Whereas the inter-muon separation expected from generic hadronic interactions high in the atmosphere is typically of $\mathcal{O}(5-10\text{ m})$, neutrino-induced multi-W phenomena occur primarily inside the Earth and result in much more spatially compact muon bundles.

Figure 19 compares MACRO data for pair-wise muon separation to the contribution expected from neutrino-induced multi-W phenomena for ($\sqrt{\hat{s}_0} = 2.4\text{ TeV}$, $\hat{\sigma}_0 = 10\ \mu\text{b}$). The MACRO data is taken from Fig. 4 of ref. [65] and corresponds to muon bundles at zenith angles $\theta < 60^\circ$ detected by two supermodules operating for 2334.3 hours. The MACRO data contains contributions from muon bundles of all multiplicities; approximately half of the reconstructed pairs come from $n_\mu = 2$ muon bundles. We suggest that by separately examining the pair-wise muon separation in bundles with fixed numbers of muons (*e.g.*, $n_\mu=3$) as has been done the Fréjus collaboration [66], MACRO may be able to put constraints on the existence of multi-W phenomena. A particularly useful signature of multi-W processes in this respect is the energy carried by each muon. Muons arising from multi-W processes in Fig. 19 would have energies of approximately 80 TeV as they

³Preliminary rates for muon bundles in MACRO presented in ref. [64] included only AGN ν_μ -induced multi-W processes and hence are smaller than those of fig. 18 by a factor of 3.

enter the detector and may be distinguished by mechanisms such as catastrophic energy loss [62, 63]. Though some of the region in $(\sqrt{\hat{s}_0}, \hat{\sigma}_0)$ space to which MACRO is sensitive is already excluded by the Fly’s Eye (assuming the same AGN neutrino flux), valuable independent constraints may already be possible from existing MACRO data.

5 Summary and Conclusions

Future hadron colliders such as the proposed SSC or LHC offer the best prospects for observing or constraining multi-W phenomena. A naive measure of an experiment’s sensitivity to multi-W phenomena is the size of the region in $(\sqrt{\hat{s}_0}, \hat{\sigma}_0)$ parameter space accessible to the experiment by requiring at least one multi-W event in 10^7 s of operation. By this standard the SSC covers the most territory (see Fig. 2). For example, at the SSC one would expect $\mathcal{O}(100 \text{ events} / 10^7 \text{ s})$ if multi-W processes were characterized by $(\sqrt{\hat{s}_0} = 20 \text{ TeV}, \hat{\sigma}_0 = 1 \text{ pb})$. Even in the relatively noisy environment of a high-luminosity hadron collider, the spectacular signature of $\gtrsim \mathcal{O}(30)$ gauge bosons in a single event has no conceivable Standard Model background. In this sense, when applied to a hadron collider, even a naive measure of the sensitivity to multi-W phenomena is appropriate.

Before the commissioning of hadron supercolliders, cosmic ray physics suggests alternative techniques for searching for multi-W processes induced either by protons or neutrinos. Taken at face value, the most optimistic cosmic ray constraints on multi-W phenomena come from 1) the non-observation of neutrino-induced air showers by Fly’s Eye (see Fig. 12) which covers the full range of $\sqrt{\hat{s}_0}$ up to 40 TeV if $\hat{\sigma}_0 \gtrsim \mathcal{O}(10 - 100 \text{ nb})$ and 2) searches for horizontal muon bundles in DUMAND (see Fig. 16) whose sensitivity extends to $\hat{\sigma}_0 \simeq \mathcal{O}(1 \text{ nb})$ if $\sqrt{\hat{s}_0} \lesssim \mathcal{O}(4 \text{ TeV})$. Additional constraints on neutrino-induced phenomena may be forthcoming from limits on the occurrence of energetic, spatially compact non-horizontal muon bundles in MACRO or,

more speculatively, from large energy deposits in proposed acoustic arrays.

Understandably, none of the neutrino-based constraints presented in this paper are conclusive: all presume the existence of a sizeable flux of ultrahigh energy neutrinos from AGN or neutrinos photoproduced off the 2.7 K cosmic background radiation. If it should happen the required neutrino flux is absent, no conclusions may be drawn regarding the existence of multi-W processes — one would then have to wait for the advent of supercolliders to observe or exclude multi-W phenomena. However, it is instructive to consider an intermediate scenario in which a flux of ultrahigh energy neutrinos is detected in the future but is found to have interactions consistent generic charged current processes; this too may place constraints on the existence of exotic phenomena. In any case, since no experiment has yet studied the interactions of neutrinos with energies greater than a few hundred GeV, it may be premature to dismiss the possibility that PeV neutrinos have novel interactions.

To avoid the additional uncertainty of whether an ultrahigh energy neutrino flux exists, we have also considered the possibility of multi-W phenomena induced by a cosmic protons. Unfortunately, the tradeoff for a relatively reliable proton flux is an overwhelming competing cross section due to generic hadronic processes. Large competing cross sections complicate matters in two ways. First, they drastically reduce the proton flux effectively available for multi-W phenomena. Even by our naive measure of sensitivity to multi-W phenomena, a 100 km² surface array operating for 10⁷ s could only see multi-W phenomena if $\sqrt{\hat{s}_0} \lesssim \mathcal{O}(10 - 12 \text{ TeV})$ and $\hat{\sigma}_0 \gtrsim \mathcal{O}(0.1 - 1 \mu\text{b})$ (see, *e.g.*, Fig. 3). Second, large competing cross sections are the source of an overwhelming background of generic air showers. Given that there are optimistically $\mathcal{O}(10^4 - 10^5)$ generic showers for every shower of multi-W origin, we have emphasized that multi-W showers could easily be mistaken for background fluctuations. Taking this difficulty into consideration, the true sensitivity of conventional surface arrays to proton-induced multi-W phenomena is

negligible. Similar conclusions apply to other techniques for proton-induced multi-W phenomena such as detecting downward moving underground TeV muons in MACRO, or searching for the anomalous longitudinal development of air showers with the Fly's Eye.

The short term outlook for constraining or detecting multi-W phenomena in cosmic ray physics is mixed. Without making additional assumptions (such as assuming the existence of a large cosmic neutrino flux) one must focus on proton-induced processes and conclude that current and future experiments are effectively insensitive to multi-W phenomena over the entire range of parameter space where they might plausibly exist. From this viewpoint one must wait for terrestrial supercolliders before conclusive constraints on multi-W processes are established. While this conservative scenario may very well be true, an exciting alternative exists. If a sizeable flux of cosmic neutrinos is present, not only may AMANDA, DUMAND, MACRO, NESTOR and NT-200 be sensitive to them through generic weak interactions, but such detectors may also indicate whether multi-W processes are real or an artifact of our imperfect understanding of multi-TeV weak interactions.

6 Acknowledgements

We would like to thank the following individuals for their advice and assistance during the course of this work: P. Biermann, S. Billers, C. Bloise, J. Cobb, M. Goodman, G. Heinzlmann, P. Litchfield, H. Meyer, S. Mrenna, A. Shoup, F. Stecker, and R. Vázquez. We appreciate the aide of the UC Irvine Physics Group. D.A.M. acknowledges the hospitality of the CERN theory group during a productive visit. D.A.M. is supported by the Eloisatron project.

7 Appendix

In this appendix we outline our quantitative description of multi-W processes. In sect. 7.1 we state the assumptions and approximations used to model proton-induced multi-W production and in sect. 7.2 we briefly describe our simulation of extensive air showers. Finally, in sect. 7.3 we review the calculation of subsurface detection rates for muon bundles from neutrino-induced multi-W processes.

7.1 Proton-induced multi-W processes

Within our working hypothesis the proton-nucleon multi-W cross section is given by

$$\sigma_{\text{multi-W}}^{pN} = \sum_{ij} \int dx_1 dx_2 \frac{f_i(x_1) f_j(x_2) + f_i(x_2) f_j(x_1)}{1 + \delta_{ij}} \hat{\sigma}_0 \Theta \left(\sqrt{x_1 x_2 s} - \sqrt{\hat{s}_0} \right), \quad (12)$$

where $f_i(x)$ is the parton distribution function corresponding to a parton of flavour i carrying a proton momentum fraction x . The sum extends over all distinct⁴ combinations of quarks and antiquarks (but not gluons). We evaluate all parton distribution functions at a scale $Q^2 = M_W^2$ and employ the leading-order parton distributions of Tung and Morfin (fit SL) [67].

In the proton-nucleon center of momentum system (c.m.s.) where the total energy is \sqrt{s} , we sample the parton distribution functions to generate the momentum fractions x_1, x_2 carried by the quarks participating in the hard interaction. In the quark-quark c.m.s. the energy of the hard subprocess is $\sqrt{\hat{s}} = \sqrt{x_1 x_2 s}$. For definiteness we assume that multi-W processes

⁴Equation 12 corrects eq. 3 of ref. [13]. Though ref. [13] used eq. 12 for calculations, the $\sigma_{\text{multi-W}}^{pp}$ curve in Fig. 1 of ref. [13] is too large by approximately a factor of 2 due to an incorrect double-counting of contributions from unlike partons.

produce exactly 30 W bosons. A more detailed scenario should consider the production of Z bosons (roughly in the ratio $W^+ : W^- : Z \simeq 1 : 1 : 1$), prompt Higgs bosons, prompt photons and allow for fluctuations in the total weak boson multiplicity. In addition, we should, strictly speaking, ensure the conservation of the quantum numbers carried by the quarks participating in the hard interaction by allowing more than W bosons in the final state of the hard subprocess. In the interest of simplicity we will sacrifice complete consistency and forgo such refinements; compared to the large number of gauge bosons produced we do not expect these points to play a significant role in our investigation of whether or not it is feasible to observe multi-W processes.

We assume that in the quark-quark c.m.s. the W boson momenta are distributed isotropically with each W boson carrying an energy $\sqrt{\hat{s}}/30$. A more detailed treatment should employ 30-body relativistic phase space and perhaps impose dynamic assumptions such as limited $p_T \simeq \mathcal{O}(m_W)$ of the W bosons (in analogy with limited p_T in QCD). However, because of the rapidly falling parton-parton luminosity, the quark-quark subprocess energy $\sqrt{\hat{s}}$ tends to lie just above the multi-W threshold $\sqrt{\hat{s}_0}$. Consequently, for multi-W thresholds close to the kinematic limit for the production of 30 W bosons (*i.e.*, $\sqrt{\hat{s}_0} \simeq 2.4$ TeV) there is little extra energy available to have to worry about the precise distribution of the W bosons in momentum space.

We employ the Monte Carlo program JETSET [68] to decay all W bosons and to reproduce measured W branching fractions and hadronic multiplicities. At this stage we inhibit the decays of relatively long-lived secondaries such as $\pi^\pm, \kappa^\pm, \rho, \eta, \kappa_L, \eta'$ to allow for the possibility that they may undergo hadronic interactions with air nuclei in the subsequent air shower. The extensive air shower simulator described in sect. 7.2 will determine whether these secondaries decay or interact.

Aside from the decays of the W bosons we must also consider those parts of the colliding protons which do not participate in the hard subprocess

— the so-called spectator fragments. Since the quarks participating in the subprocess carry colour, the hadronization of the spectator fragments is not, in general, independent of the hadronization of the subprocess system. As a simplification we ignore this by point and adopt the following procedure: 1) We treat the multi- W production subprocess as a color singlet (and hence hadronize it independently by decaying all 30 W bosons). 2) We replace the spectator fragment originating from the cosmic proton with a nucleon carrying the same energy. 3) We ignore the spectator fragment originating from the stationary “target” proton. This ansatz, especially steps 2) and 3), is intended to embody the essential characteristics of the leading particle effect. As a final step we boost all W decay products and the leading nucleon to the Earth rest frame and inject them into the upper atmosphere to be used as initial conditions for an extensive air shower.

7.2 Air shower simulation

We use the computer program SHOWERSIM [36] to simulate both the electromagnetic and hadronic components of air showers generated by multi- W processes. The program accounts for multiple hadronic and electromagnetic interactions in the atmosphere and allows for the decay of unstable particles. The interested reader is referred to the SHOWERSIM documentation for a detailed discussion of the program’s physical assumptions. We employed the program in its default form with few exceptions. For the electromagnetic components of showers we employed the ELCAS.5 and TAIL.2 routines which provide a detailed evolution of photons and electrons below 200 GeV; for the underlying hadronic interaction model we used the “W00” option which nominally fits SPS data.

We also used SHOWERSIM to generate samples of generic air showers induced by protons and iron nuclei. We stress that though we employed SHOWERSIM exclusively, we did so only for convenience since it is not clear that

any available shower model, especially concerning the hadronic component of extensive air showers, provides an accurate representation of Nature. In this respect, our results for multi-W air showers, generic proton or iron showers may not be accurate on an absolute scale but should be reliable relative to each other due to common simulation techniques.

7.3 Multi-muon detection rates

For completeness we summarize here the ingredients of our calculations of multi-muon detection rates. The interested reader is referred to ref. [13] for additional details.

We characterize a subsurface detector by its vertical depth D , its geometrical size (length L , width W , height H) and a muon threshold energy E_{thresh} which is the minimum energy required of muon entering the detector in order that it pass completely through the detector. For our calculations we idealize DUMAND (with a nine string array) as a $100 \text{ m} \times 100 \text{ m} \times 250 \text{ m}$ volume at an ocean depth of 4.5 km with $E_{\text{thresh}} = 100 \text{ GeV}$. For simplicity we neglect the effective growth of the array size with muon energy. Similarly, we idealize MACRO as $77 \text{ m} \times 12 \text{ m} \times 9 \text{ m}$ volume located at depth of 3700 hg/cm² below the surface of a spherical Earth of density $\rho = 2.6 \text{ g/cm}^3$. For MACRO we assume $E_{\text{thresh}} = 2 \text{ GeV}$. Since prompt muons from multi-W phenomena would typically arrive at DUMAND or MACRO with energies $\gtrsim \mathcal{O}(10 \text{ TeV})$, the small values of E_{thresh} used above are essentially irrelevant.

For an isotropic differential flux of cosmic neutrinos, j_ν , the differential flux of detected events with k muons in coincidence originating from multi-W phenomena is given by

$$\frac{dN_{k\mu}}{dA dt d\Omega} = \int_{E_{\text{thresh}}}^{\infty} dE P_{k\mu}(E, X) j_\nu(E), \quad (13)$$

where the total column density of matter between the detector and the upper

atmosphere is

$$X = \rho \left[\sqrt{(R_{\oplus} - D)^2 \cos^2 \theta + 2DR_{\oplus} - D^2} - (R_{\oplus} - D) \cos \theta \right] + X_{\text{atm}}. \quad (14)$$

The first term in the column density accounts for rock/water/ice above the detector and the second term is the appropriate atmospheric slant depth using the U.S. Standard atmosphere model.

$P_{k\mu}(E, X)$ is the probability that a cosmic neutrino of energy E , initially separated from the detector by a column density X , gives rise to a multi-W event with k muons detected in coincidence,

$$P_{k\mu}(E, X) = \frac{n_{\mu}!}{(n_{\mu} - k)!k!} N_A \sigma_{\text{multi-W}}^{\nu N} \int_0^X dX' e^{-N_A \sigma_{\text{tot}}^{\nu N} (X - X')} \tilde{p}_{\mu}^k (1 - \tilde{p}_{\mu})^{n_{\mu} - k}, \quad (15)$$

where n_{μ} is the number of collimated muons produced in a multi-W event and $N_A = m_p^{-1}$. We assume $n_{\mu} = n_W/9 \simeq 3$, corresponding to prompt muons from the decay of 30 W bosons.

$\tilde{p}_{\mu}(E, E_{\text{thresh}}, X')$ is the detection probability for a typical prompt muon produced in a multi-W process induced by a neutrino with energy E . Under the assumption that the n_W weak gauge bosons are distributed isotropically in the subprocess rest frame,

$$\tilde{p}_{\mu}(E, E_{\text{thresh}}, X') = 1 - n_W \frac{E'_{\mu}(E_{\text{thresh}}, X')}{E}, \quad (16)$$

where $E'_{\mu}(E_{\text{thresh}}, X')$ is the solution of the muon energy-range relation

$$X' = \int_{E_{\text{thresh}}}^{E'_{\mu}} \frac{dE}{\alpha(E) + \beta(E)E}. \quad (17)$$

We neglect the stochastic effects of range straggling which may become important for muon energies above 10^5 GeV and use parametrizations of $\alpha(E)$ and $\beta(E)$ from refs. [69, 70], respectively.

The distribution of the inter-muon separation in muon bundles from neutrino-induced multi-W processes is obtained as a byproduct of using standard Monte Carlo techniques to evaluate the integral of eq. 11 which gives

the number of underground muon bundles. For each point contributing to the integral of eq. 11 one generates a muon bundle configuration, propagates it to the detector and calculates its contribution to the distribution of pair-wise separations using the integrand of eq. 11 as a weight. Muon bundle configurations are generated according to the assumptions outlined in sect. 7.1. Namely, for a cosmic neutrino of energy E_ν initiating a multi-W process, one samples the parton distribution functions of the target nucleon to determine the quark-neutrino c.m.s. energy $\sqrt{\hat{s}} = \sqrt{2m_p E_\nu x}$ ($> \sqrt{\hat{s}_0}$). Since prompt muons from W boson decay are distributed isotropically in the quark-neutrino c.m.s., one generates momentum vectors for three prompt muons in that frame and then boosts the results to the Earth rest frame. After including the effects of muon energy loss and multiple Coulomb scattering in the medium surrounding the detector, the $2 \leq n_\mu \leq 3$ muons reaching the detector determine $n_\mu(n_\mu - 1)/2$ pairwise separations which contribute to the muon separation distribution such as shown in fig. 19.

References

- [1] A. Ringwald, Nucl. Phys. B330 (1990) 1.
- [2] O. Espinosa, Nucl. Phys. B343 (1990) 310.
- [3] L. McLerran, A. Vainshtein and M. Voloshin, Phys. Rev. D42 (1990) 171.
- [4] J. Cornwall, Phys. Lett. B243 (1990) 271.
- [5] H. Goldberg, Phys. Lett. B246 (1990) 445.
- [6] A. Ringwald and C. Wetterich, Nucl. Phys. B353 (1991) 303; C. Wetterich, Nucl. Phys. B (Proc. suppl.) 22A (1991) 43.
- [7] M. Mattis, Phys. Rep. 214 (1992) 159; P. Tinyakov, CERN preprint CERN-TH.6708 (1992); A. Ringwald, CERN preprint CERN-TH.6862 (1993).
- [8] (Incomplete) list of papers dealing with multi-particle production in weakly coupled theories: E. Argyres, R. Kleiss and C. Papadopoulos, Nucl. Phys. B391 (1993) 42; P. Arnold and M. Mattis, Phys. Rev. D42 (1990) 1738; Mod. Phys. Lett. A6 (1991) 2059; L.S. Brown, Phys. Rev. D46 (1992) 4125; J. Cornwall and G. Tiktopoulos, Phys. Rev. D45 (1992) 2105; H. Goldberg, Phys. Rev. D45 (1992) 2945; Phys. Rev. Lett. 69 (1992) 3017; S. Khlebnikov, V. Rubakov and P. Tinyakov, Nucl. Phys. B350 (1991) 441; V.V. Khoze and A. Ringwald, Nucl. Phys. B355 (1991) 351; Phys. Lett. B259 (1991) 106; M. Maggiore and M. Shifman, Phys. Rev. D42 (1992) 3550; Nucl. Phys. B380 (1992) 22; A.H. Mueller, Nucl. Phys. B348 (1991) 310; *ibid.* B353 (1991) 44; *ibid.* B364 (1991) 109; M. Porrati, Nucl. Phys. B347 (1990) 371; A. Ringwald, Phys. Lett. B285 (1992) 113; G. Veneziano, Mod. Phys. Lett. A7 (1992) 1661; M.

- Voloshin, Nucl. Phys. B383 (1992) 233; V. Zakharov, Nucl. Phys. B353 (1991) 683; *ibid.* B371 (1992) 637; Phys. Rev. Lett. 67 (1991) 3650.
- [9] G. Farrar and R. Meng, Phys. Rev. Lett. 65 (1990) 3377.
- [10] A. Ringwald, F. Schrempp, and C. Wetterich, Nucl. Phys. B365 (1991) 3.
- [11] P. Bosetti *et al.* (DUMAND Collaboration), Hawaii DUMAND Center preprint HDC-2-88 (1989); C.M. Alexander *et al.*, in: Proc. 23rd Int. Cosmic Ray Conf., Calgary, July 1993, eds. J. Wdowczyk *et al.*, (U. of Calgary, Calgary, 1993), Vol. 4, p. 515.
- [12] L.K. Resvanis (NESTOR Collaboration), in: Proc. Workshop on High Energy Neutrino Astrophysics, Honolulu, March 1992, eds. V. Stenger, J. Learned, S. Pakvasa and X. Tata, (World Scientific, Singapore, 1993), p. 325.
- [13] D.A Morris and R. Rosenfeld, Phys. Rev. D44 (1991) 3530.
- [14] L. Bergström, R. Liotta and H. Rubinstein, Phys. Lett. B276 (1992) 231; L. Dell’Agnello *et al.*, INFN Firenze preprint DFF 178/12 (1992), to appear in: Proc. 2nd NESTOR Int. Workshop, Pylos, October 1992.
- [15] F. Stecker, C. Done, M. Salamon, and P. Sommers, Phys. Rev. Lett. 66 (1991) 2697; *ibid.* 69 (1992) 2738 (Erratum); in: Proc. Workshop on High Energy Neutrino Astrophysics, Honolulu, March 1992, eds. V. Stenger, J. Learned, S. Pakvasa and X. Tata, (World Scientific, Singapore, 1993), p. 1.
- [16] A. Szabo and R. Protheroe, in: Proc. Workshop on High Energy Neutrino Astrophysics, Honolulu, March 1992, eds. V. Stenger, J. Learned, S. Pakvasa and X. Tata, (World Scientific, Singapore, 1993), p. 24.

- [17] P. Biermann, in: Proc. Workshop on High Energy Neutrino Astrophysics, Honolulu, March 1992, eds. V. Stenger, J. Learned, S. Pakvasa and X. Tata, (World Scientific, Singapore, 1993), p. 86; L. Nellen, K. Mannheim, and P. Biermann, Bonn preprint TK-92-08 (1992).
- [18] For a review see: V. Stenger, DUMAND preprint DUMAND-9-92 (1992), to appear in: Proc. 2nd NESTOR Int. Workshop, Pylos, October 1992.
- [19] S. Barwick *et al.* (AMANDA Collaboration), in: Proc. 26th Int. Conf. on High Energy Physics, Dallas, August 1992, ed. J.R. Sanford, (AIP, New York, 1993) Vol. 2, p. 1250.
- [20] S. Ahlen *et al.* (MACRO Collaboration), Nucl. Instr. Meth. A324 (1993) 337.
- [21] I. Sokalski and Ch. Spiering (eds.) (The Baikal Collaboration), Baikal preprint BAIKAL 92-03 (1992); in: Proc. 23rd Int. Cosmic Ray Conf., Calgary, July 1993, eds. J. Wdowczyk *et al.*, (U. of Calgary, Calgary, 1993), Vol. 4, p. 573.
- [22] N. Manton, Phys. Rev. D28 (1983) 2019; Klinkhamer and N. Manton, Phys. Rev. D30 (1984) 2212.
- [23] N. Chiba *et al.* (AGASA Collaboration) Nucl. Instr. Meth. A311 (1992) 338.
- [24] D. Alexandreas *et al.* (CYGNUS Collaboration), Nucl. Instr. Meth. A311 (1992) 350.
- [25] K. Gibbs (CASA Collaboration), Nucl. Instr. Meth. A264 (1988) 67; R. Ong, Nucl. Phys. B (Proc. suppl.) 14A (1990) 273.

- [26] M. Aglietta *et al.* (EAS-TOP Collaboration), Nucl. Instr. Meth. A277 (1989) 23.
- [27] G.E. Khristiansen *et al.* (EAS-100 Collaboration), in: Proc. 23rd Int. Cosmic Ray Conf., Calgary, July 1993, eds. J. Wdowczyk *et al.*, (U. of Calgary, Calgary, 1993), Vol. 4, p. 287.
- [28] O. Allkofer, M. Samorski, and W. Stamm (HEGRA Collaboration), in: NATO Advanced Workshop on Very High Energy Gamma Ray Astronomy, Durham, 1986, ed. K.E. Turver (Reidel, Dordrecht, 1987), p. 281; F. Aharonian *et al.* in: Proc. 23rd Int. Cosmic Ray Conf., Calgary, July 1993, eds. J. Wdowczyk *et al.*, (U. of Calgary, Calgary, 1993), Vol. 4, p. 291.
- [29] K. Bekk *et al.* (KASCADE Collaboration), in: Proc. 23rd Int. Cosmic Ray Conf., Calgary, July 1993, eds. J. Wdowczyk *et al.*, (U. of Calgary, Calgary, 1993), Vol. 4, p. 674.
- [30] G. Bari (LVD Collaboration), Nucl. Instr. Meth. A277 (1989) 11.
- [31] J. Thron (Soudan-2 Collaboration), Nucl. Instr. Meth. A283 (1989) 642.
- [32] R. Baltrusaitis *et al.* (Fly's Eye Collaboration), Nucl. Instr. Meth. A240 (1985) 410.
- [33] J. Kempa and J. Wdowczyk, J. Phys. G9 (1983) 1271.
- [34] J. Linsley, in: Proc. 18th Int. Cosmic Ray Conf., Bangalore, August 1983, eds. N. Durgaprasad *et al.*, (Tata Institute, Bombay, 1983), Vol. 12, p. 135; C. Fitchel and J. Linsley, Astrophys. J. 300 (1986) 474.
- [35] R. Ren *et al.*, Phys. Rev. D38 (1988) 1404.
- [36] J.A. Wrontniak, SHOWERSIM/84, U. of Maryland report 85-191 (1985), (unpublished); update, April 1990 (unpublished).

- [37] P. Sokolsky, Introduction to Ultrahigh Energy Cosmic Ray Physics (Addison-Wesley, Reading, 1989).
- [38] V. Berezhinskii and A. Gazizov, Yad. Fiz. 33 (1981) 230 [Sov. J. Nucl. Phys. 33 (1981) 120].
- [39] F. Wilczek, Phys. Rev. Lett. 55 (1985) 1252.
- [40] V. Berezhinskii, in Neutrino '77: Proc. Int. Conf. on Neutrino Physics and Neutrino Astrophysics, Baksan Valley, June 1977, (Nauka, Moscow, 1978); D. Eichler, Astrophys. J. 232 (1979) 106; R. Silberberg and M. Shapiro, in: Proc. 16th Int. Cosmic Ray Conf., Kyoto, 1979, (University of Tokyo, Tokyo, 1979), Vol. 10, p. 357; V. Berezhinskii and V. Ginzburg, Mon. Not. Roy. Astron. Soc. 194 (1981) 3.
- [41] V. Berezhinskii *et al.*, Astrophysics of Cosmic Rays (North-Holland, Amsterdam, 1990).
- [42] D. Kazanas and D. Ellison, Astrophys. J. 304 (1986) 178.
- [43] K. Mannheim, in: Proc. Workshop on High Energy Neutrino Astrophysics, Honolulu, March 1992, eds. V. Stenger, J. Learned, S. Pakvasa and X. Tata, (World Scientific, Singapore, 1993), p. 105.
- [44] F. Stecker, private communication.
- [45] T.J. Turner and K.A. Pounds, Mon. Not. R. Astr. Soc. 240 (1989) 833; K. Pounds *et al.*, Nature 344 (1990) 132.
- [46] P. Biermann, private communication.
- [47] F.W. Stecker, A.K. Harding and J.J. Barnard, Nature 316 (1985) 418; T.K. Gaisser, F.W. Stecker, A.K. Harding and J.J. Barnard, Astrophys. J. 309 (1986) 674; J. MacDonald, T. Stanev and P. Biermann, Astrophys. J. 378 (1991) 30.

- [48] R. Baltrusaitis *et al.* (Fly's Eye Collaboration), Phys. Rev. D31 (1985) 2192.
- [49] J. MacGibbon and R. Brandenberger, Nucl. Phys. B331 (1990) 153.
- [50] R. Baltrusaitis *et al.* (Fly's Eye Collaboration), Nucl. Instr. Meth. A264 (1988) 87.
- [51] K. Greisen, Phys. Rev. Lett. 16 (1966) 748; G. Zatsepin and V.A. Kuzmin, Pis'ma Zh. Eksp. Teor. Fiz. 4 (1966) 53 [JETP Lett. 4 (1966) 78].
- [52] V. Berezhinskii and G. Zatsepin, in: Proc. 1976 DUMAND Workshop, Honolulu, September 1976, ed. A. Roberts (Fermilab, Batavia, 1976) p. 15; in: Proc. 15th Int. Cosmic Ray Conference, Plovdiv, Bulgaria, August 1977, (Bulgarian Academy of Sciences, Sofia, 1977) p. 248; V. Berezhinsky and L. Ozernoy, Astron. Astrophys. 98 (1981) 50.
- [53] C. Hill and D. Schramm, Phys. Lett. B131 (1983) 247; Phys. Rev. D31 (1985) 564.
- [54] S. Mrenna, Phys. Rev. D45 (1992) 2371.
- [55] G. Domokos and S. Nussinov, Phys. Lett. B187 (1987) 372; G. Domokos and S. Kovesi-Domokos, Phys. Rev. D38 (1988) 2833.
- [56] M. Nagano *et al.*, J. Phys. Soc. Japan 30 (1971) 33; M. Nagano *et al.*, J. Phys. G12 (1986) 69.
- [57] F. Halzen and E. Zas, Phys. Lett. B289 (1992) 184; E. Zas, F. Halzen, and R.A. Vázquez, in: Proc. 23rd Int. Cosmic Ray Conf., Calgary, July 1993, eds. J. Wdowczyk *et al.*, (U. of Calgary, Calgary, 1993), Vol. 4, p. 434.

- [58] R.A. Vázquez, private communication.
- [59] S. Karaevsky *et al.* (SADCO Collaboration), in: Proc. 23rd Int. Cosmic Ray Conf., Calgary, July 1993, eds. J. Wdowczyk *et al.*, (U. of Calgary, Calgary, 1993), Vol. 4, p. 550.
- [60] P.B. Price, Nucl. Instr. and Meth. A325 (1993) 346.
- [61] J. Learned, Phys. Rev. D19 (1979) 3293; J. Learned and R.J. Wilkes, in: Proc. 23rd Int. Cosmic Ray Conf., Calgary, July 1993, eds. J. Wdowczyk *et al.*, (U. of Calgary, Calgary, 1993), Vol. 4, p. 538.
- [62] H. Meyer (Fréjus Collaboration), in: Proc. of the XXVIIth Rencontre de Moriond, Les Arcs, Savoie, France, January 1992, eds. G. Chardin, O. Fackler and J. Tran Thanh Van (Ed. Frontières, Gif-sur-Yvette, 1992) p. 169.
- [63] W. Allison *et al.* (Soudan-2 Collaboration), in: Proc. Workshop on High Energy Neutrino Astrophysics, Honolulu, March 1992, eds. V. Stenger, J. Learned, S. Pakvasa and X. Tata, (World Scientific, Singapore, 1993), p. 243.
- [64] D.A. Morris and A. Ringwald in: Proc. 23rd Int. Cosmic Ray Conf., Calgary, July 1993, eds. J. Wdowczyk *et al.*, (U. of Calgary, Calgary, 1993), Vol. 4, p. 407.
- [65] S. Ahlen *et al.* (MACRO Collaboration), Phys. Rev. D46 (1992) 4836.
- [66] Ch. Berger *et al.* (Fréjus collaboration), Phys. Rev. D40 (1989) 2163.
- [67] J.G. Morfin and W.K. Tung, Z. Phys. C 52 (1991) 13.
- [68] T. Sjostrand, CERN preprint CERN-TH.6488 (1992).

- [69] L. Bezrukov and E. Bugaev, in: Proc. DUMAND Summer Workshops at Khabarovsk and Lake Baikal, 1979, ed. J. Learned (Hawaii DUMAND Center, Honolulu, 1980), p. 227.
- [70] A. Kalinosvkii, N. Mokhov, and Yu. Nikitin, Passage of High-Energy Particles Through Matter (AIP, New York, 1989).

Figure Captions

1. Universal curves parametrizing multi-W production cross sections in proton-nucleon (pN), proton-electron (pe^-), neutrino-nucleon (νN) and neutrino-electron (νe^-) collisions. Curves are for protons and neutrinos with laboratory energy E colliding with nucleons and electrons at rest. $E_p^{(pN \text{ thresh})} = \hat{s}_0/(2m_p)$ is the proton threshold energy for pN multi-W processes. The (pN) curve corrects an error in ref. [13]; the corresponding curve of ref. [13] is too large by approximately a factor of 2 (see footnote in appendix).
2. Contours corresponding to 1 and 10 multi-W events in one year (10^7 s) of operation for the LHC ($\mathcal{L} = 10^{34} \text{ cm}^{-2} \text{ s}^{-1}$) and the SSC ($\mathcal{L} = 10^{33} \text{ cm}^{-2} \text{ s}^{-1}$).
3. Event number contours in 10^7 s for proton-induced multi-W air showers assuming the Constant Mass Composition model for proton flux. Solid: 100 km^2 conventional surface array sensitive to $E_{\text{shower}} \geq 1 \text{ PeV}$ at zenith angles $\theta \leq 60^\circ$. Dashed: Fly's Eye array sensitive to $E_{\text{shower}} \geq 100 \text{ PeV}$ using aperture of ref. [32].
4. Differential flux of protons and neutrinos used in text. The Constant Mass Composition proton flux is from ref. [33]. The diffuse neutrino flux from active galactic nuclei (AGN) and the 2.7 K photoproduced neutrino flux are taken from ref. [15]. Neutrino fluxes shown are summed over species in the proportion $\nu_\mu : \bar{\nu}_\mu : \nu_e : \bar{\nu}_e = 2 : 2 : 1 : 1$.
5. Differential flux of proton-induced multi-W air showers assuming the Constant Mass Composition (CMC) model proton flux for fixed multi-W production parameters.
6. Lateral distributions of electrons ($E_e > 1 \text{ MeV}$), muons ($E_\mu > 1 \text{ GeV}$) and hadrons ($E_{\text{had}} > 1 \text{ GeV}$) in 5 PeV vertical air showers (lower

three curves in each plot) and 30 PeV vertical air showers (upper three curves in each plot) at atmospheric depth of 800 g/cm². Solid curves correspond to proton-induced multi-W showers assuming $\sqrt{\hat{s}_0} = 2.4$ TeV and any value of $\hat{\sigma}_0$. Dashed (dot-dashed) curves correspond to generic showers initiated by proton (iron) primaries. Each curve is an average over 25–100 showers including variations in the depth of first interaction.

7. Average fraction of total shower energy E_p carried by generic component of a proton-induced multi-W air shower. $E_p^{\text{thresh}} = \hat{s}_0/(2m_p)$ is the proton threshold energy for multi-W production.
8. Lateral distributions of muons with $E_\mu > 1.5$ TeV at atmospheric depth of 800 g/cm² for vertical air showers initiated by 30 PeV primaries. The multi-W processes assume $\sqrt{\hat{s}_0} = 2.4$ TeV. Each curve is an average over 100–500 showers including variations in the depth of first interaction.
9. Longitudinal development curves for 150 PeV hadron-induced vertical air showers. The depths of first interaction are fixed at 42 g/cm² for p-induced multi-W showers, 42 g/cm² for generic p-initiated showers and 11 g/cm² for generic Fe-initiated showers. A multi-W parton-parton threshold of $\sqrt{\hat{s}_0} = 5$ TeV is assumed. A number of curves are shown to illustrate the similarity between multi-W showers and fluctuations in generic showers.
10. Neutrino interaction length due to combined effects of generic charged current interactions and multi-W processes.
11. Excluded region (hatched) in $E_\nu - \sigma_{\text{tot}}^{\nu N}$ space from combination (solid line) of Fly’s Eye limits with the AGN neutrino flux of Stecker *et al.* [15]. Dashed lines indicate limiting cases of $\sigma_{\text{tot}}^{\nu N}$ for ($\sqrt{\hat{s}_0} = 8$ TeV, $\hat{\sigma}_0 =$

.5 μb) and ($\sqrt{\hat{s}_0} = 8 \text{ TeV}, \hat{\sigma}_0 = 81 \mu\text{b}$) which are consistent with the Fly’s Eye limits.

12. Regions of multi-W parameter space excluded by the Fly’s Eye. The region labelled “AGN ν ” is excluded if one assumes only the AGN neutrino flux of Stecker *et al.* [15]. The region labelled “2.7 Photoproduced ν ” is excluded in addition if one includes the neutrino flux contributions due to the cosmic background radiation shown in Fig. 4.
13. Excluded regions in $E_\nu - \sigma_{\text{tot}}^{\nu N}$ space from combination (solid line) of Fly’s Eye limits with the AGN neutrino flux of Stecker *et al.* [15] (hatched) and the flux due to the 2.7 K cosmic background radiation (double hatched) (c.f. Fig. 4). Dashed lines indicate limiting cases of $\sigma_{\text{tot}}^{\nu N}$ for ($\sqrt{\hat{s}_0} = 8 \text{ TeV}, \hat{\sigma}_0 = 48 \text{ nb}$) and ($\sqrt{\hat{s}_0} = 8 \text{ TeV}, \hat{\sigma}_0 = 81 \mu\text{b}$) which are consistent with the limits.
14. Event number contours for neutrino-induced multi-W extensive air showers ($E_{\text{shower}} \geq 100 \text{ PeV}$, zenith angle $\leq 60^\circ$) in 10^7 s for a 100 km^2 conventional surface array (vertical depth 1000 g/cm^2). Solid contours includes all showers. Dashed contours include only showers initiated a minimum of 500 g/cm^2 away from array. The AGN neutrino flux of Stecker *et al.* [15] is assumed.
15. Contours for neutrino-induced contained events in 1 km^3 volume of water at an ocean depth of 4.5 km in 10^7 s (approximately the arrangement of the proposed SADC0 acoustic detector). The neutrino flux of Stecker *et al.* [15] is assumed (see Fig. 4).
16. Contours for neutrino-induced multi-W muon bundles at zenith angles $\theta > 80^\circ$ in 10^7 s at MACRO and DUMAND assuming the AGN neutrino flux of Stecker *et al.* [15].

17. Contours for neutrino-induced multi-W muon bundles for all zenith angles in 10^7 s at DUMAND assuming the AGN neutrino flux of Stecker *et al.* [15] (see Fig. 4).
18. Contours for neutrino-induced multi-W muon bundles for all zenith angles in 10^7 s at MACRO assuming the AGN neutrino flux of Stecker *et al.* [15].
19. MACRO pairwise muon separation data [65] compared with expectations for neutrino-induced multi-W phenomena for ($\sqrt{\hat{s}_0} = 2.4$ TeV , $\hat{\sigma}_0 = 10 \mu\text{b}$) assuming the AGN neutrino flux of Stecker *et al.* [15]. MACRO data corresponds to two supermodules operating for 2334.3 hours sensitive to bundles with zenith angle $\theta < 60^\circ$.

Table 1 Average particle multiplicity at atmospheric depth of 800 g/cm² for vertical extensive air showers generated by 5 PeV (and 30 PeV) primaries. Multi-W showers are proton-induced. Showers labelled p and Fe contain only generic interactions.

Shower Type	$\langle N_e \rangle$ $E_e > 1 \text{ MeV}$	$\langle N_\mu \rangle$ $E_\mu > 1 \text{ GeV}$	$\langle N_{\text{had}} \rangle$ $E_{\text{had}} > 1 \text{ GeV}$	$\langle N_\mu \rangle$ $E_\mu > 1.5 \text{ TeV}$
multi-W	1.1×10^6 (1.4×10^7)	5.9×10^4 (1.9×10^5)	2.2×10^3 (1.4×10^5)	18 (40)
p	2.4×10^6 (1.8×10^7)	4.5×10^4 (1.5×10^5)	2.9×10^3 (1.5×10^5)	5 (20)
Fe	1.3×10^6 (1.1×10^7)	8.7×10^4 (3.3×10^5)	3.3×10^3 (1.4×10^5)	14 (60)

This figure "fig1-1.png" is available in "png" format from:

<http://arxiv.org/ps/hep-ph/9308269v1>

This figure "fig1-2.png" is available in "png" format from:

<http://arxiv.org/ps/hep-ph/9308269v1>

This figure "fig1-3.png" is available in "png" format from:

<http://arxiv.org/ps/hep-ph/9308269v1>

This figure "fig1-4.png" is available in "png" format from:

<http://arxiv.org/ps/hep-ph/9308269v1>

This figure "fig1-5.png" is available in "png" format from:

<http://arxiv.org/ps/hep-ph/9308269v1>

This figure "fig1-6.png" is available in "png" format from:

<http://arxiv.org/ps/hep-ph/9308269v1>

This figure "fig1-7.png" is available in "png" format from:

<http://arxiv.org/ps/hep-ph/9308269v1>

This figure "fig1-8.png" is available in "png" format from:

<http://arxiv.org/ps/hep-ph/9308269v1>

This figure "fig1-9.png" is available in "png" format from:

<http://arxiv.org/ps/hep-ph/9308269v1>

This figure "fig1-10.png" is available in "png" format from:

<http://arxiv.org/ps/hep-ph/9308269v1>

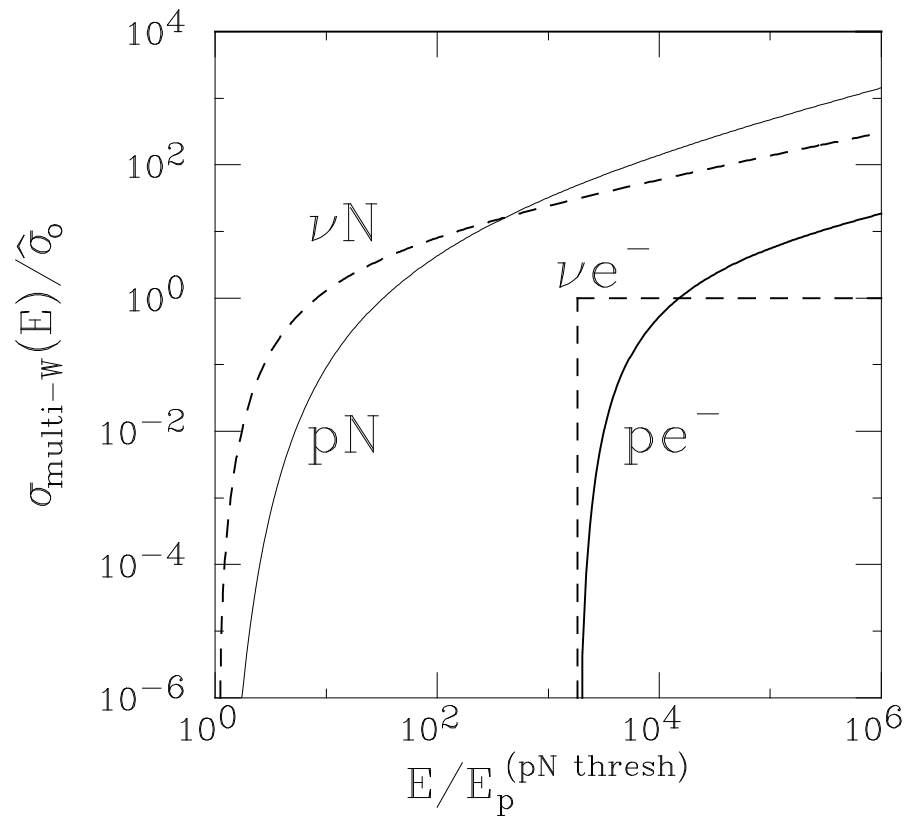


Figure 1

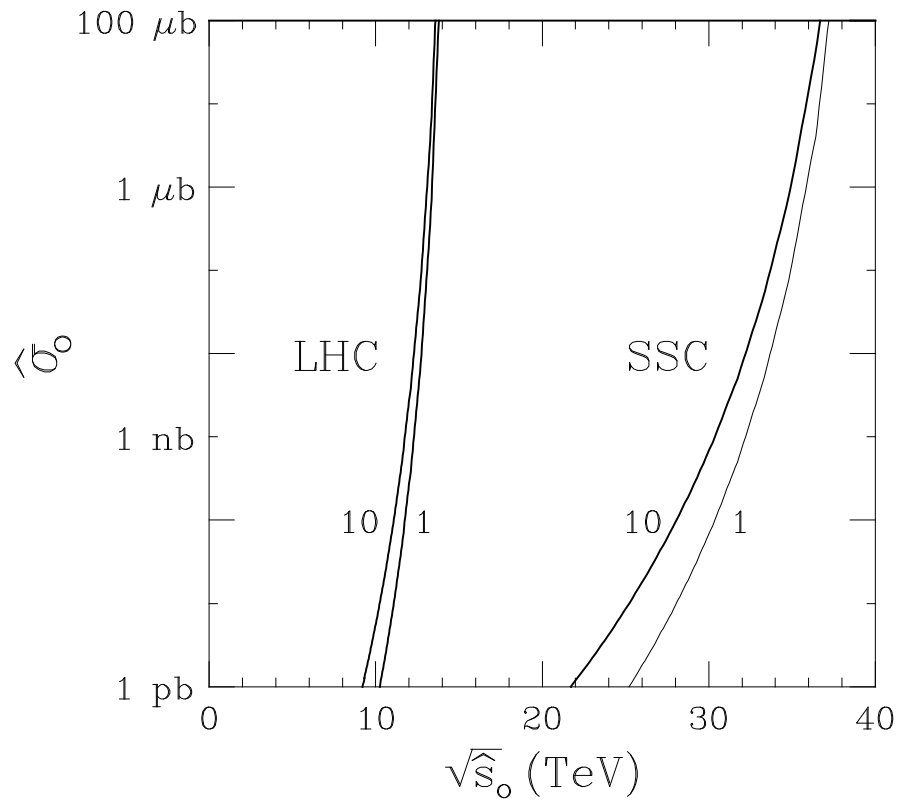


Figure 2

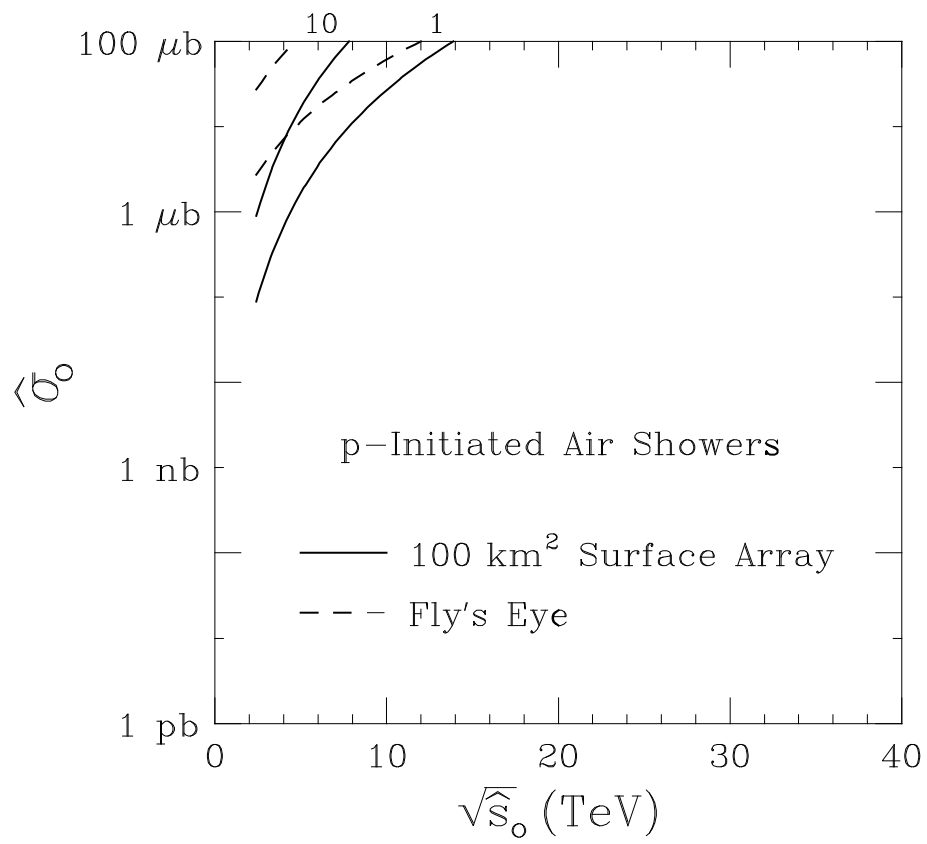


Figure 3

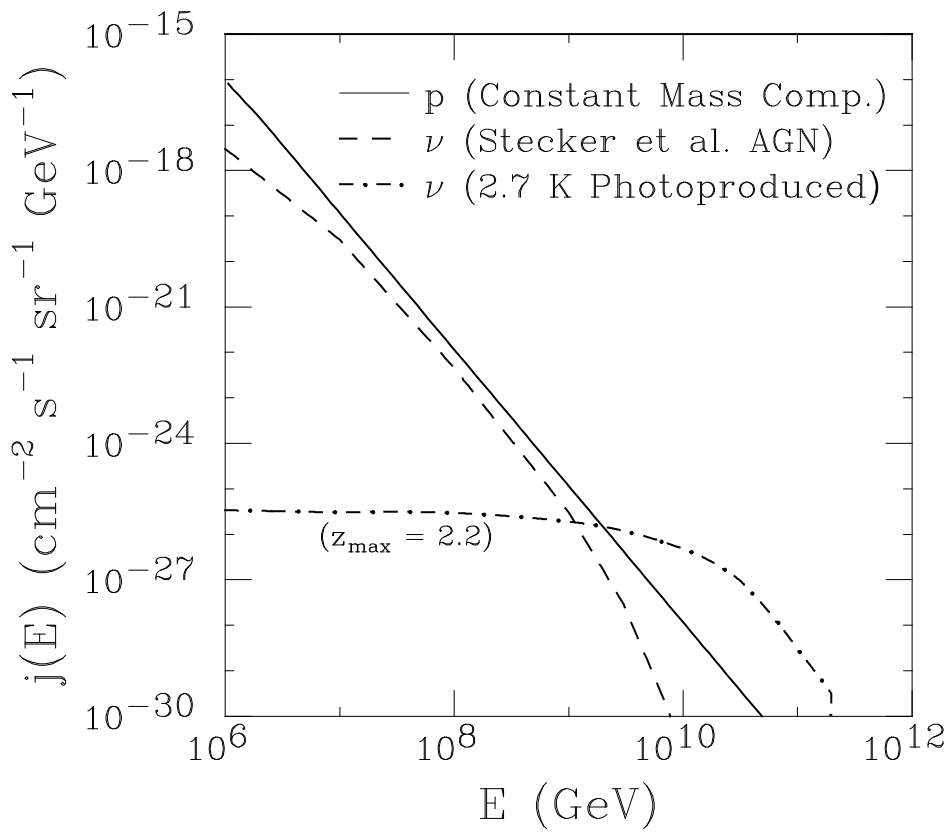


Figure 4

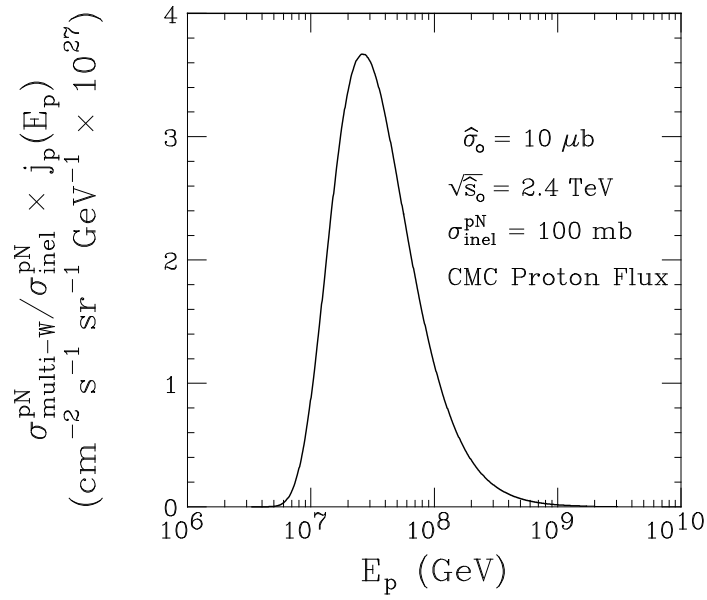


Figure 5

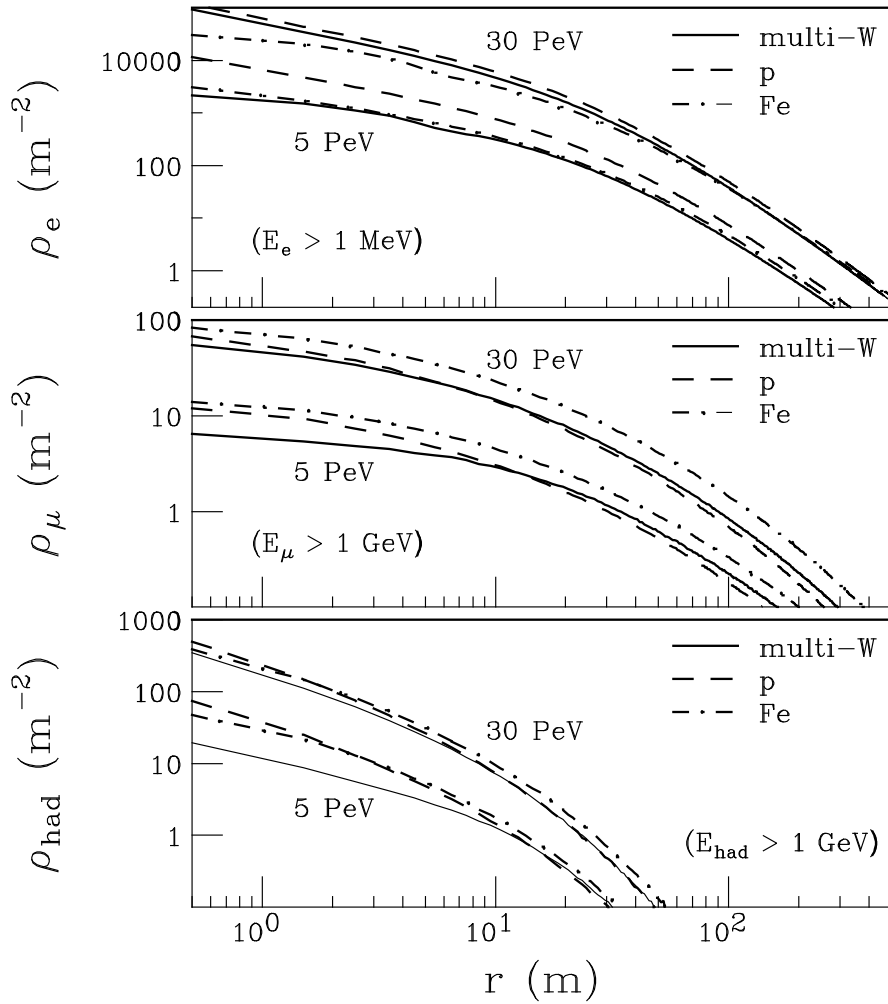


Figure 6

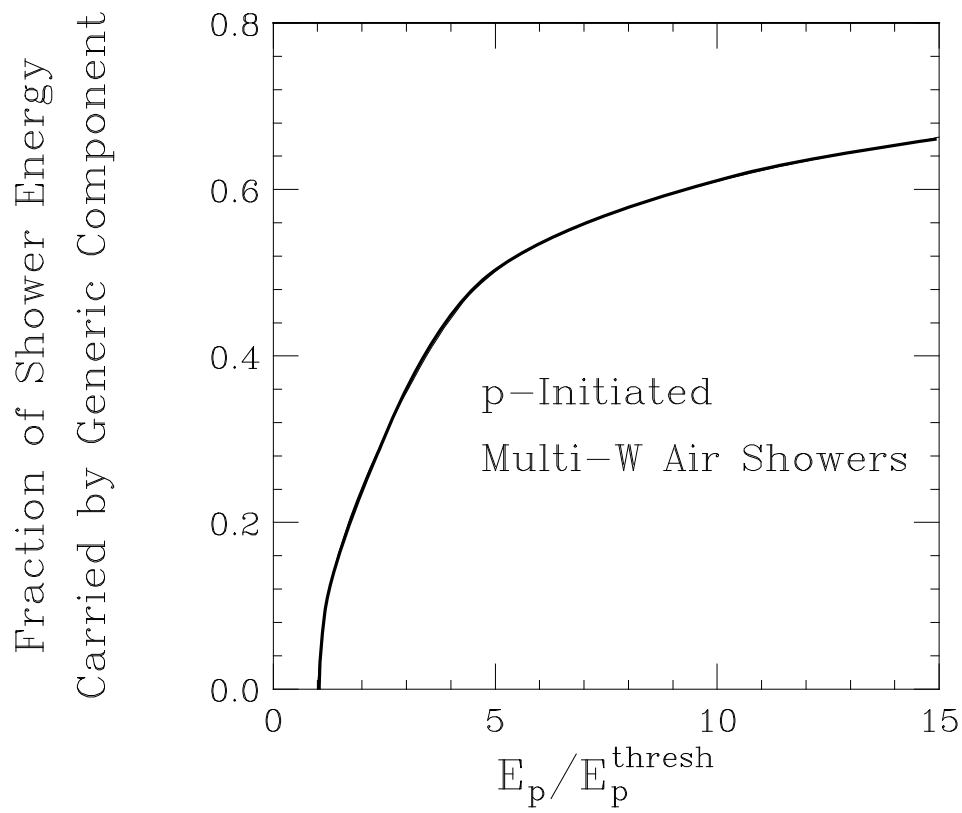


Figure 7

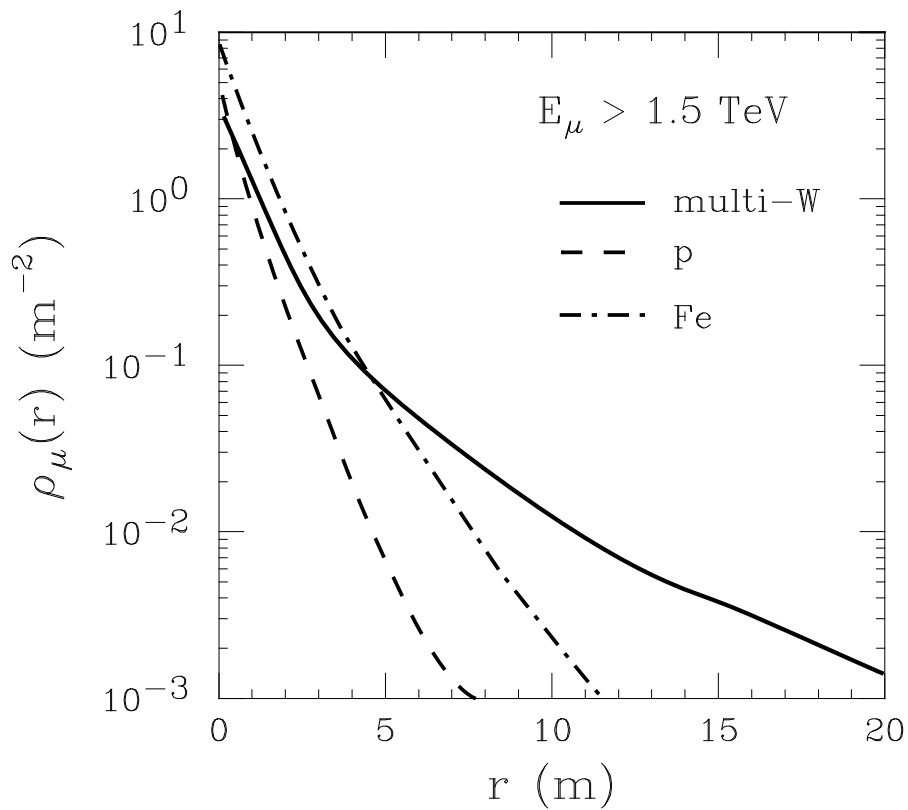


Figure 8

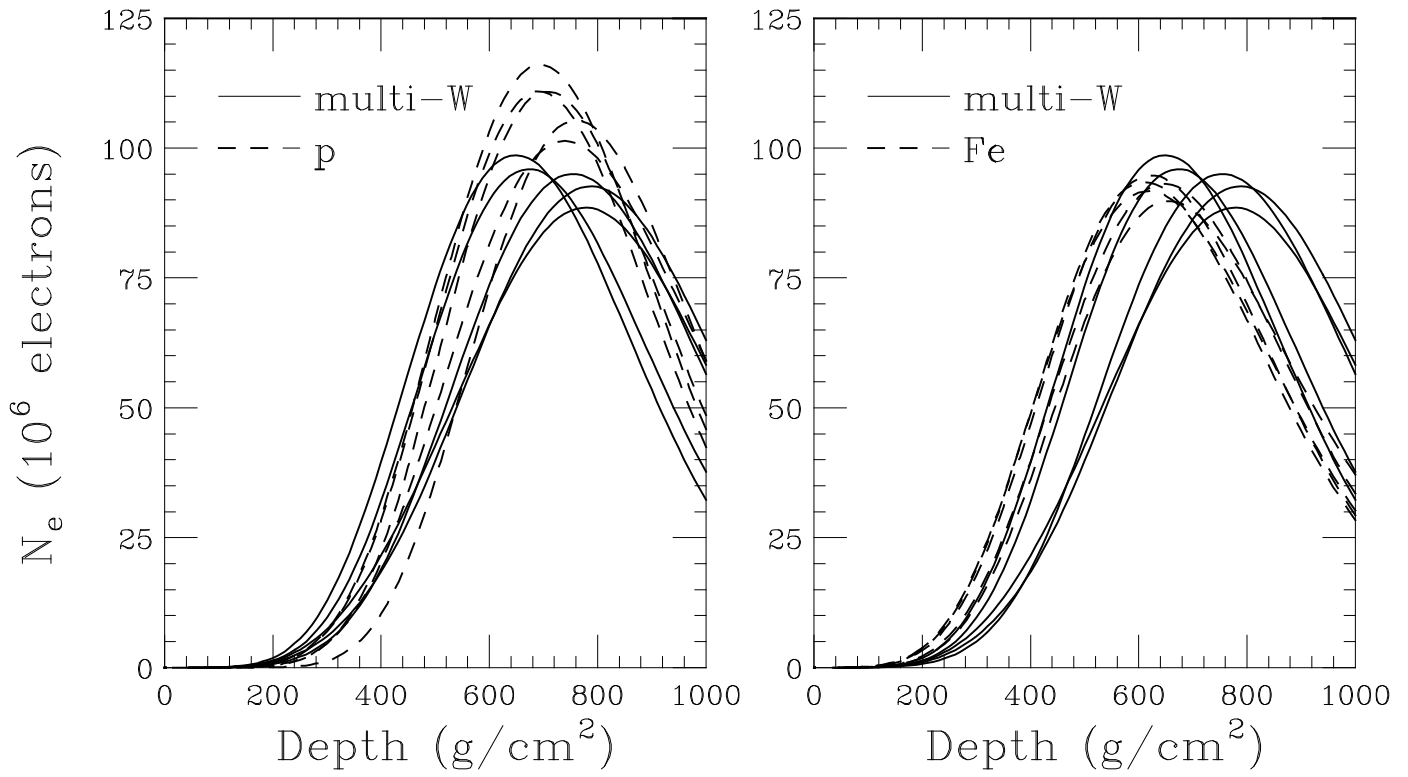


Figure 9

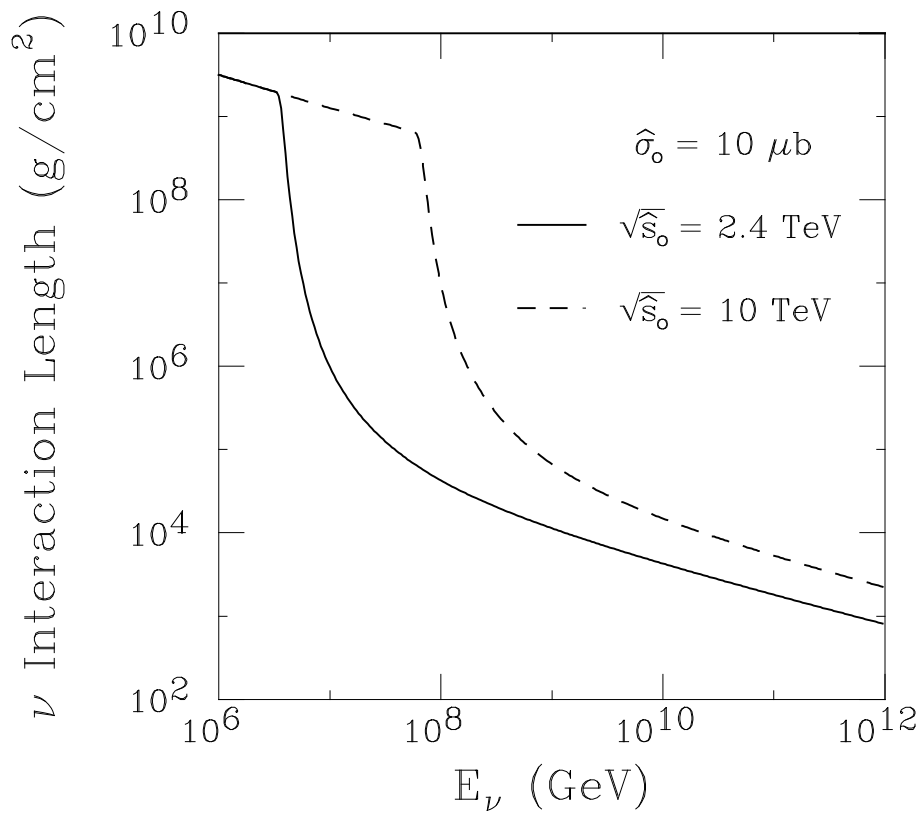


Figure 10

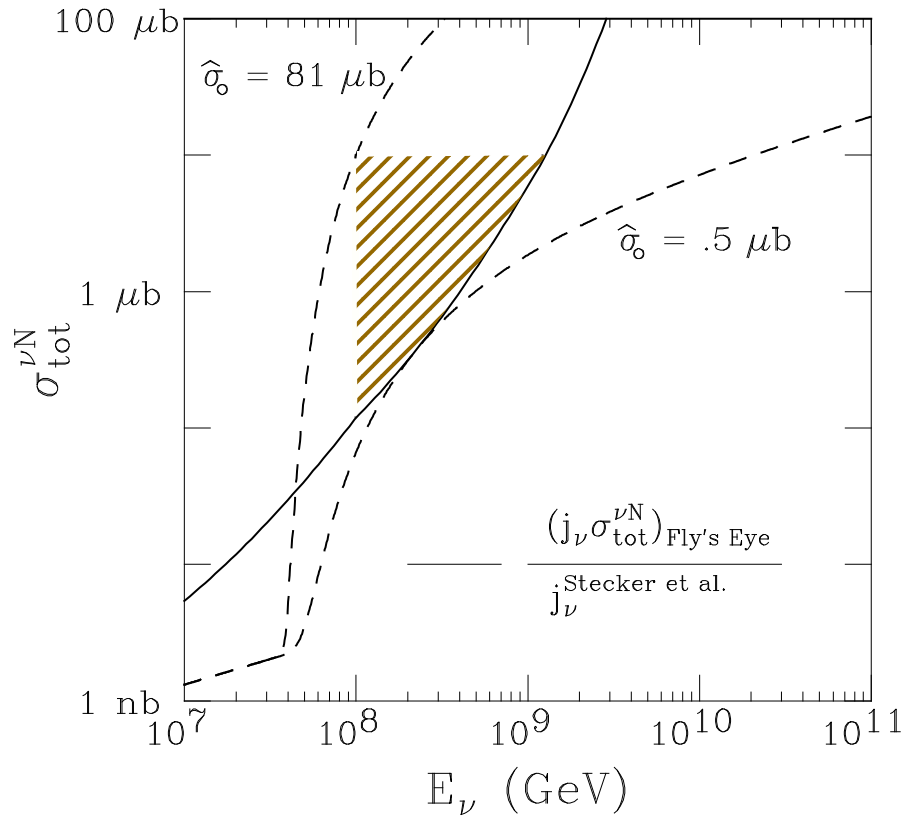


Figure 11

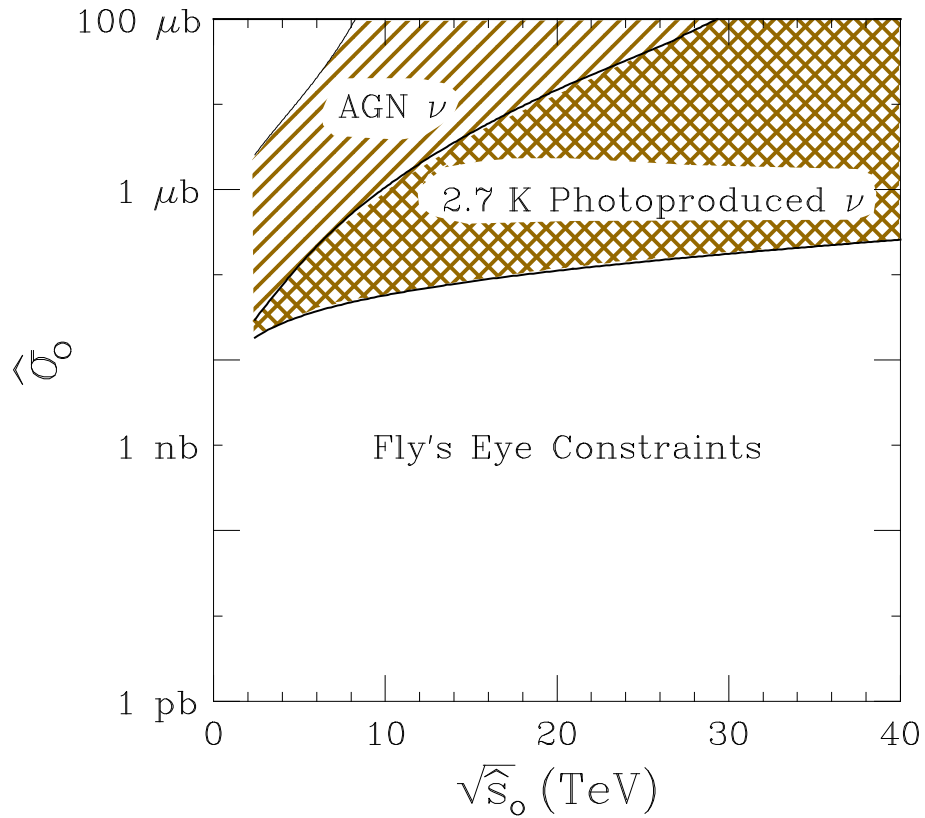


Figure 12

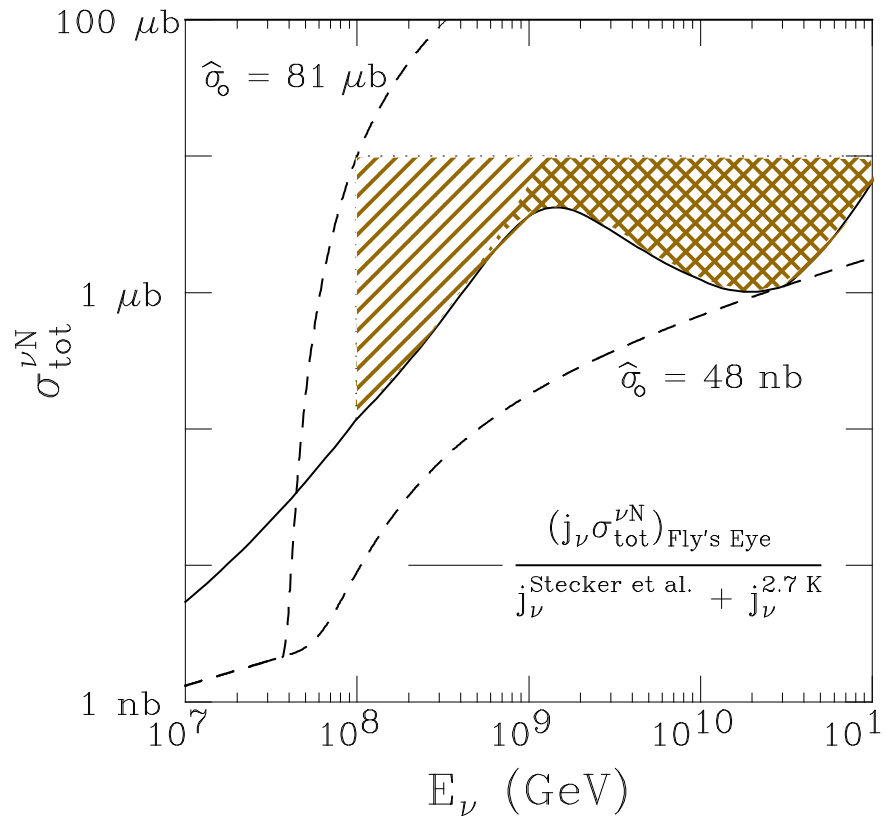


Figure 13

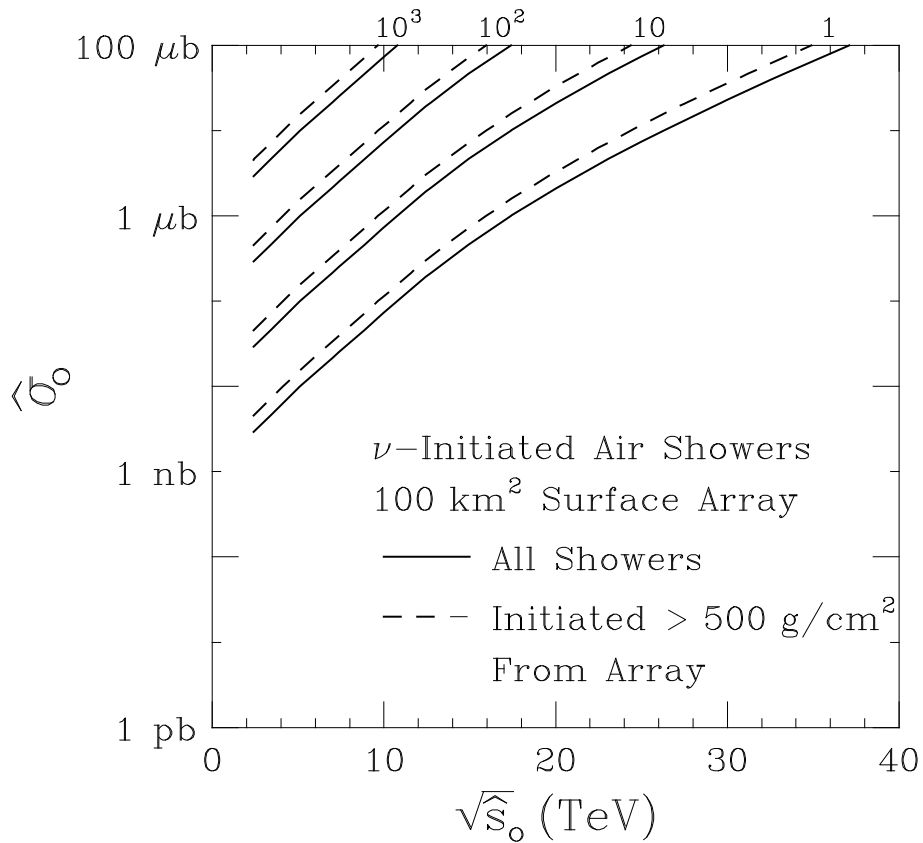


Figure 14

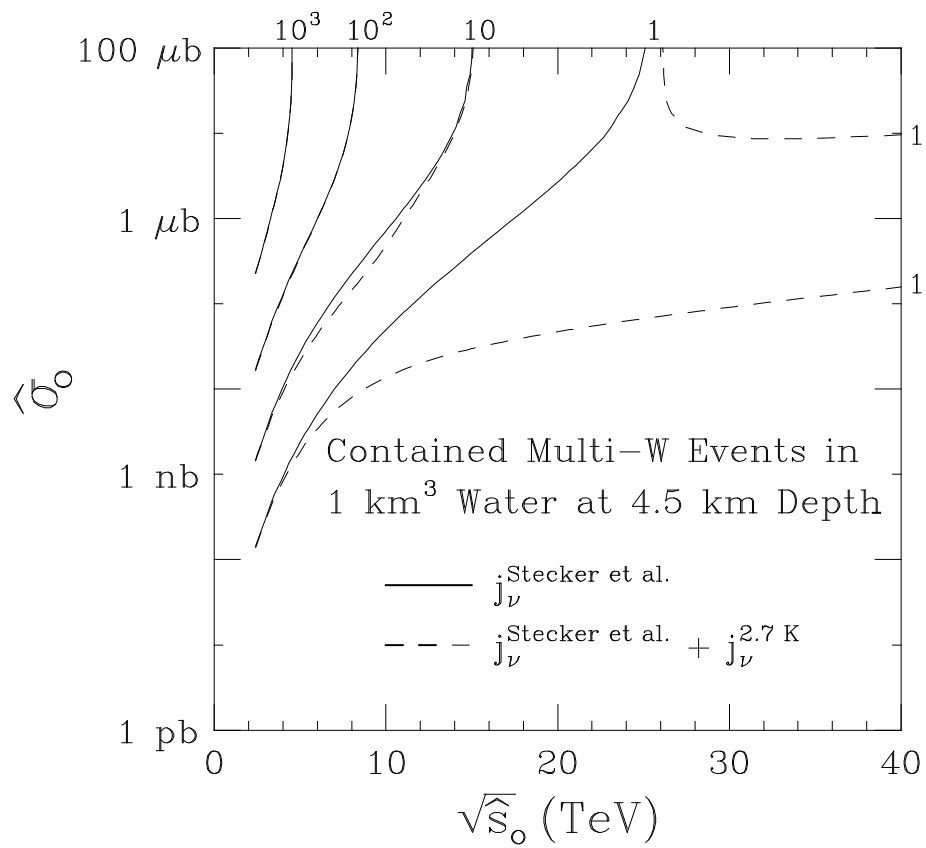


Figure 15

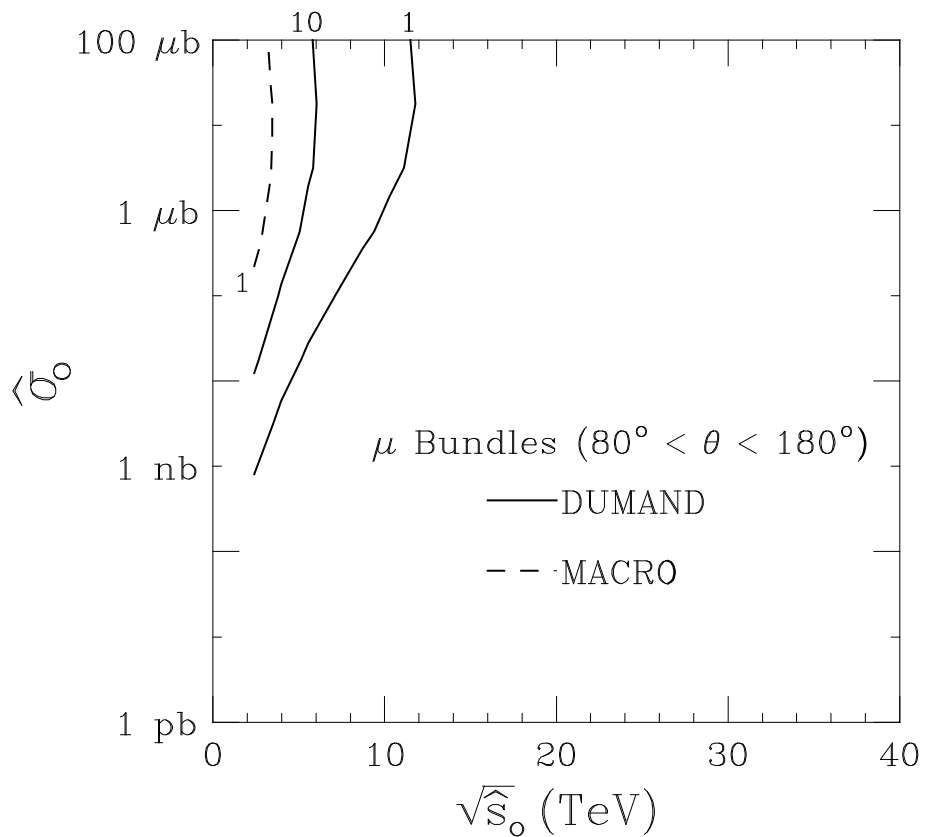


Figure 16

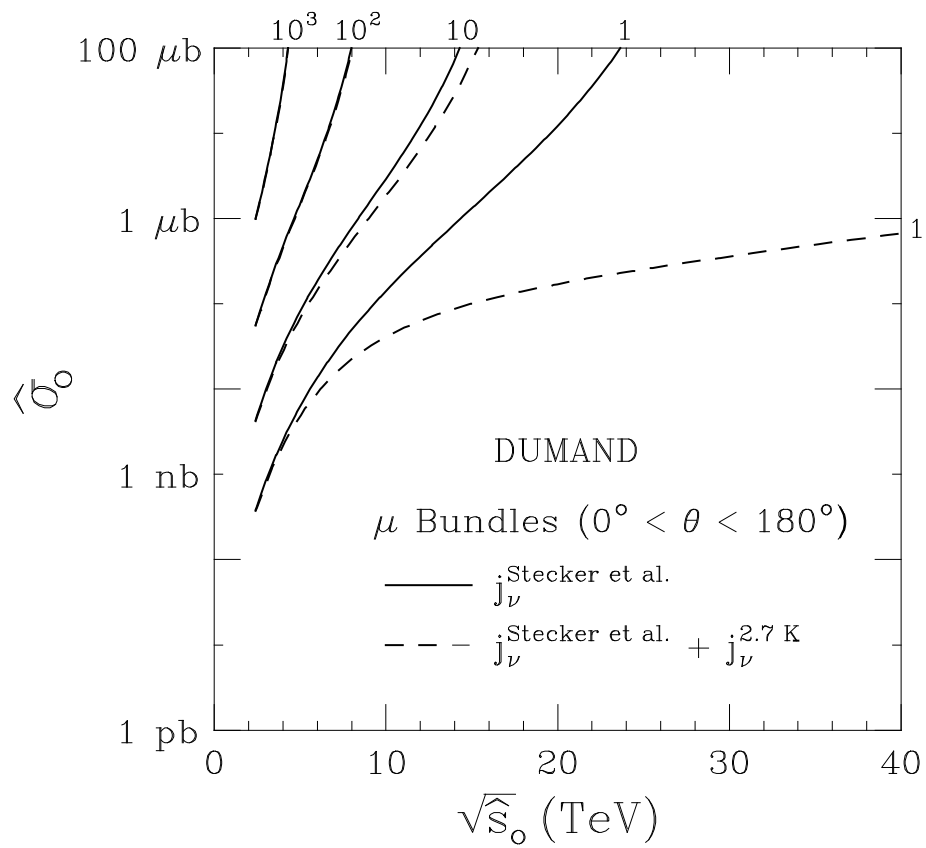


Figure 17

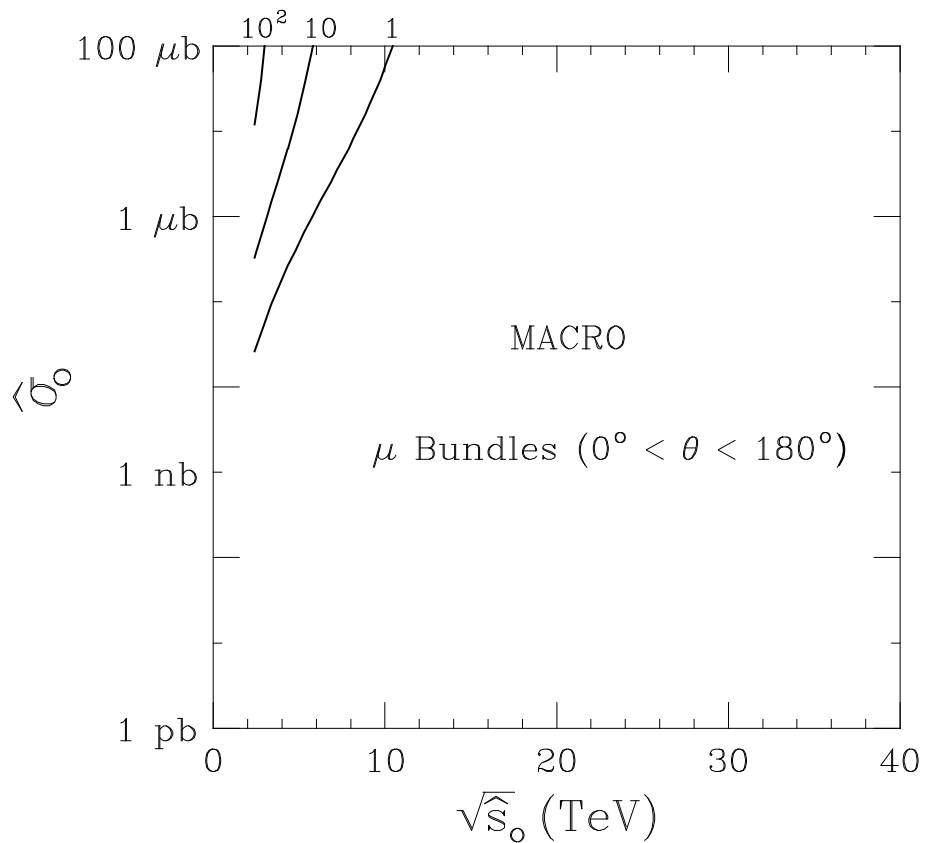


Figure 18

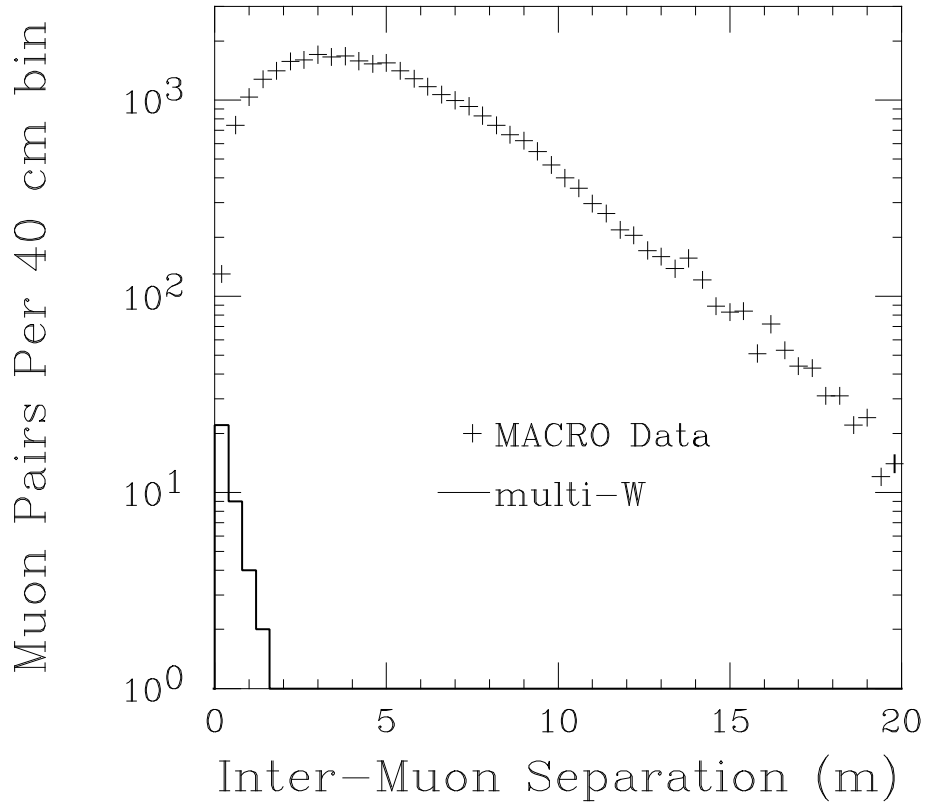


Figure 19